

Generalized squirming motion of a sphere

On Shun Pak · Eric Lauga

Received: 15 October 2013 / Accepted: 30 January 2014 / Published online: 7 May 2014
© Springer Science+Business Media Dordrecht 2014

Abstract A number of swimming microorganisms, such as ciliates (*Opalina*) and multicellular colonies of flagellates (*Volvox*), are approximately spherical in shape and swim using beating arrays of cilia or short flagella covering their surfaces. Their physical actuation on the fluid may be mathematically modeled as the generation of surface velocities on a continuous spherical surface—a model known in the literature as squirming, which has been used to address various aspects of the biological physics of locomotion. Previous analyses of squirming assumed axisymmetric fluid motion and hence required all swimming kinematics to take place along a line. In this paper we generalize squirming to three spatial dimensions. We derive analytically the flow field surrounding a spherical squirmer with arbitrary surface motion and use it to derive its three-dimensional translational and rotational swimming kinematics. We then use our results to physically interpret the flow field induced by the swimmer in terms of fundamental flow singularities up to terms decaying spatially as $\sim 1/r^3$. Our results will make it possible to develop new models in biological physics, in particular in the area of hydrodynamic interactions and collective locomotion.

Keywords Low-Reynolds-number locomotion · Squirming motion · Stokes flows

1 Introduction

Due to their small sizes, microorganisms inhabit a world where viscous forces dominate and inertial effects are negligible. The Reynolds number, which characterizes the relative importance of inertial to viscous forces, ranges typically from 10^{-5} for the smallest bacteria up to 10^{-2} for spermatozoa [1]. Fluid-based locomotion of microorganisms is vital in a number of biological processes, including reproduction, locating nutrient sources, preying, and escaping from predation [2–4]. Physically, locomotion at low Reynolds numbers suffers from the constraints due to the absence of inertia, mathematically manifested by the linearity and time independence of the governing

O. S. Pak
Department of Mechanical and Aerospace Engineering, Princeton University,
Olden Street, Princeton, NJ 08544-5263, USA
e-mail: opak@princeton.edu

E. Lauga (✉)
Department of Applied Mathematics and Theoretical Physics, University of Cambridge
Centre for Mathematical Sciences, Wilberforce Road, Cambridge CB3 0WA, UK
e-mail: e.lauga@damtp.cam.ac.uk

equation—the Stokes equations [5]. Purcell illustrated the difficulties encountered in small-scale locomotion by introducing his scallop theorem [6], which states that no reciprocal motion (body deformation possessing a time-reversal symmetry) can lead to net propulsion at zero Reynolds number [7].

Nature showcases a variety of mechanisms by which it is possible to overcome the constraints of the theorem and achieve micropropulsion. Many cells use one or more appendages, called flagella (singular: flagellum), for propulsion. Traveling waves are then propagated along the flagellum either by internal bending (seen, for example, in the spermatozoon of eukaryotic cells) or passive rotation of a rigid helical flagellum (the case of swimming bacteria), in both cases making it possible to break the time-reversal symmetry and hence escape from the constraints of the scallop theorem [5]. A number of microorganisms possess multiple flagella. *Escherichia coli* is a bacterium with a few helical flagella that can wrap into a bundle to move the cell forward when the motor turns in a specific direction. *Chlamydomonas reinhardtii* is an alga (eukaryotic cell) with two flagella. Ciliates such as *Opalina* and *Paramecium* (illustrated in Fig. 1a) and colonies of flagellates such as *Volvox* (shown in Fig. 1b) have their surface covered by arrays of cilia (or short flagella) beating in a coordinated fashion [1].

Over the past 60 years, theoretical and experimental studies on the locomotion of microorganisms have improved our understanding of life under the microscope [1,5,10]. Topics of recent active interest include the locomotion of cells in environments with complex geometries [11–13] and complex fluids [14–17], the role of motility in the formation of biofilms [18–21], the collective dynamics of active particles [22,23], and the effect of Brownian noise on swimming [24–26]. Considerable attention has also been devoted to the design of artificial microscopic swimmers [27] for potential biomedical applications such as microsurgery and targeted drug delivery [28].

Historically, Taylor [29] pioneered the theoretical modeling of flagellar hydrodynamics by analyzing the motion of a waving sheet in Stokes flows. The propulsion speed of the sheet was solved asymptotically in the limit of a small waving amplitude compared to its wavelength. Subsequently, most of the theoretical studies in the field have derived their results asymptotically, meaning they are physically valid only in specific mathematical limits: small amplitudes [14,15,29,30], long wavelengths [31,32], slender filaments [33–38], or in the far field [21,39]. As a result, very few exact solutions for swimming in Stokes flows exist.

The most popular exact solution is originally due to Lighthill [40] and Blake [41] and was developed to address the propulsion of ciliates. In their model, sometimes referred as the envelope model, the motion of closely packed cilia tips are modeled as a continuously deforming surface (envelope) over the body of the organism, taken to be of spherical shape [40,41]. The deformation of the envelope can then be expanded about the surface of the spherical cell body, and to leading order the action of the cilia is represented by distributions of radial and tangential velocities on the spherical surface. Lighthill [40] first derived the exact solution to the Stokes equation due to such a squirming motion on a sphere, with subsequent corrections and generalizations by Blake [41]. Since then, the squirmer model has been all but adopted as the hydrogen atom of low-Reynolds-number swimming. Originally developed to specifically model the swimming of ciliates, the squirmer model can also be useful in the study of other types of swimming microorganisms, broadly categorized as “pushers” and “pullers” [5]. Pushers obtain their thrust from the rear part of their body, such as the swimming of all peritrichous bacteria (like *E. coli*). In contrast, for pullers the thrust comes from their front part, such as the breaststroke swimming of algae genus *Chlamydomonas*. The

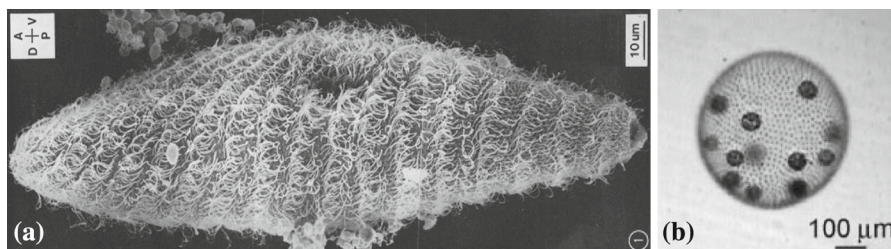


Fig. 1 **a** Ciliary motion of *Paramecium* [8]. **b** Flagellar motion of *Volvox* [9]. All images were reprinted with permission: **a** from Tamm [8] Copyright 1972 Rockefeller University Press; **b** from Solari et al. [9] Copyright 2006 National Academy of Sciences of the United States of America

squirming model can represent pushers and pullers by correspondingly changing the surface actuation (squirming profile), rendering it a general model for investigating the locomotion of microorganisms. As such, it has been used to study many problems including the hydrodynamic interactions of swimmers [42, 43], suspension dynamics [44, 45], nutrient transport and uptake by microorganisms [46–48], optimal locomotion [49], and non-Newtonian [50, 51] and inertial effects [52].

Most studies on squirming motion follow the notation of Lighthill [40] and Blake [41] and assume that the surface distortion is axisymmetric. This simplifies the analysis significantly and results in swimmers undergoing swimming along their axis of symmetry only. Real microorganisms, however, actuate the fluid in a nonaxisymmetric fashion. The protozoan *Paramecium*, for instance, rotates as it swims and has a helical distribution of cilia (Fig. 1a). Stone and Samuel [53] derived formulae that relate the translational and rotational velocities of a squirmer to the arbitrary squirming profiles on the sphere via the reciprocal theorem. In experiments with *V. carteri*, Drescher et al. [54] measured nonaxisymmetric squirming profiles and utilized these reciprocal relations to analyze the swimming kinematics of the cell. However, the reciprocal relations give no information on the flow surrounding the squirmer.

In this paper, we generalize the classical squirming results to nonaxisymmetric actuation. Using Lamb's general solution in Stokes flow [55], we derive analytically the exact solution for the flow field surrounding the swimmer, together with the swimming kinematics, for a general nonaxisymmetric squirmer. Lamb's general solution is ideally suited for problems with spherical or nearly spherical [56] geometries, and a detailed description of the solution and its applications can be found in classical textbooks [57, 58]. Our results will be useful for addressing the role of nonaxisymmetric actuation in a variety of problems in the biological physics of locomotion, including feeding and sensing, and the rheology of active suspensions. Furthermore, from a fundamental fluids perspective, our study makes it possible to establish a link between arbitrary surface motion and the appearance of nonaxisymmetric flow singularities.

The structure of the paper is as follows. The problem is mathematically formulated in Sect. 2, followed by a summary of the axisymmetric case in Sect. 3, where the swimming kinematics (Sect. 3.1) and flow structure (Sect. 3.2) are presented. We then generalize the analysis to a nonaxisymmetric squirmer in Sect. 4, where we present the swimming kinematics (Sects. 4.1 and 4.2), the three-dimensional flow structure (Sect. 4.3), the rate of work due to swimming (Sect. 4.4), and the decomposition of arbitrary surface velocities in the form of Lamb's general solution (Sect. 4.5). We conclude in Sect. 5. In Appendix A, we include detailed expressions of the flow singularities used throughout the paper. While in the main text we present the results of a squirmer with purely tangential deformation, we include the more general case of a nonaxisymmetric squirmer with radial deformation in Appendices B–D.

2 Formulation

We model theoretically the motion of a spherical ciliate of radius a in an incompressible fluid at zero Reynolds number using spherical coordinates (Fig. 2), with \mathbf{e}_r , \mathbf{e}_θ , and \mathbf{e}_ϕ as the basis vectors. Following the envelope model, the action of the cilia is represented by a general squirming profile (tangential and radial surface velocities) over the spherical surface at $r = a$. The fluid around the squirmer is governed by the Stokes equations

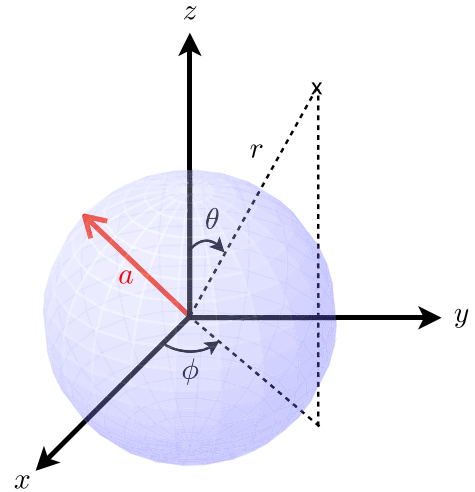
$$\eta \nabla^2 \mathbf{u} = \nabla p, \quad (1)$$

and the continuity equation for incompressible flows

$$\nabla \cdot \mathbf{u} = 0, \quad (2)$$

where $\mathbf{u} = u_r \mathbf{e}_r + u_\theta \mathbf{e}_\theta + u_\phi \mathbf{e}_\phi$ and p represent the velocity and pressure fields, respectively, and η denotes the dynamic viscosity of the fluid. In the main text, we present only the results in the case of purely tangential squirming motion (i.e., no radial surface velocities), $u_r(r = a, \theta, \phi) = 0$, because it is the most widely used squirming model in the literature. For completeness the more general case, which includes the radial deformation, is presented in Appendices B and C.

Fig. 2 Geometrical setup of a spherical squirmer of radius a . Using spherical coordinates, we denote the radial coordinate, the polar, and azimuthal angles by r , θ , and ϕ , respectively



A general solution to the Stokes equations can be obtained by constructing the homogeneous (\mathbf{u}_H) and particular (\mathbf{u}_P) solutions. The homogenous solution can be constructed as [55,57,58]

$$\mathbf{u}_H = \nabla\Phi + \nabla \times (\mathbf{r}\chi), \quad (3)$$

where \mathbf{r} is the position vector, and Φ and χ are both harmonic functions

$$\nabla^2\Phi = \nabla^2\chi = 0. \quad (4)$$

One can expand the functions Φ and χ in series of solid spherical harmonics, $\Phi = \sum_{n=-\infty}^{\infty} \Phi_n$ and $\chi = \sum_{n=-\infty}^{\infty} \chi_n$, where Φ_n and χ_n denote spherical harmonics of order n as

$$\Phi_n = r^n \sum_{m=0}^n P_n^m(\mu)(b_{mn} \cos m\phi + \tilde{b}_{mn} \sin m\phi), \quad (5)$$

$$\chi_n = r^n \sum_{m=0}^n P_n^m(\mu)(c_{mn} \cos m\phi + \tilde{c}_{mn} \sin m\phi). \quad (6)$$

Here $\mu = \cos \theta$ and $P_n^m(\mu)$ are the associated Legendre polynomials [59,60] of order m and degree n , defined as solutions to the linear differential equation for $f(\mu)$

$$\frac{d}{d\mu} \left[(1 - \mu^2) \frac{df}{d\mu} \right] + \left[n(n+1) - \frac{m^2}{1 - \mu^2} \right] f = 0. \quad (7)$$

By taking the divergence of Eq. (1) and utilizing the continuity equation, Eq. (2), we obtain that the pressure satisfies the Laplace equation $\nabla^2 p = 0$. The pressure is therefore also harmonic, and we can again expand it in a series of solid spherical harmonics, $p = \sum_{n=-\infty}^{\infty} p_n$, where

$$p_n = r^n \sum_{m=0}^n P_n^m(\mu)(a_{mn} \cos m\phi + \tilde{a}_{mn} \sin m\phi). \quad (8)$$

One can then use these results to construct a particular solution to the Stokes equation as

$$\mathbf{u}_P = \sum_{n=-\infty}^{\infty} \left[\frac{(n+3)r^2 \nabla p_n}{2\eta(n+1)(2n+3)} - \frac{n\mathbf{r}p_n}{\eta(n+1)(2n+3)} \right], \quad (9)$$

where $r = |\mathbf{r}|$ denotes the magnitude of the position vector.

Superimposing the homogenous and particular solutions gives the general solution

$$\mathbf{u} = \sum_{n=-\infty}^{\infty} \left[\frac{(n+3)r^2 \nabla p_n}{2\eta(n+1)(2n+3)} - \frac{n\mathbf{r}p_n}{\eta(n+1)(2n+3)} + \nabla\Phi_n + \nabla \times (\mathbf{r}\chi_n) \right], \quad (10)$$

usually named after Lamb [55].

Here we require that the solution must decay at infinity ($r \rightarrow \infty$), and hence all harmonics of positive order are discarded. In addition, following Brenner [56], we replace n by $-(n + 1)$ in Eq. (10) to obtain the form of Lamb’s solution convenient for exterior problems,

$$\mathbf{u}(r, \theta, \phi) = \sum_{n=1}^{\infty} \left[-\frac{(n-2)r^2 \nabla p_{-n-1}}{2\eta n(2n-1)} + \frac{(n+1)\mathbf{r}p_{-n-1}}{\mu n(2n-1)} + \nabla \Phi_{-n-1} + \nabla \times (\mathbf{r}\chi_{-n-1}) \right], \tag{11}$$

where

$$p_{-n-1} = r^{-n-1} \sum_{m=0}^n P_n^m (A_{mn} \cos m\phi + \tilde{A}_{mn} \sin m\phi), \tag{12}$$

$$\Phi_{-n-1} = r^{-n-1} \sum_{m=0}^n P_n^m (B_{mn} \cos m\phi + \tilde{B}_{mn} \sin m\phi), \tag{13}$$

$$\chi_{-n-1} = r^{-n-1} \sum_{m=0}^n P_n^m (C_{mn} \cos m\phi + \tilde{C}_{mn} \sin m\phi), \tag{14}$$

and the pressure field is given by $p = \sum_{n=1}^{\infty} p_{-n-1}$. Notice that the solutions of the case $n = 0$ have also been discarded since they correspond to sources and sinks, which are unphysical in problems related to rigid particles [40,41,58].

After performing all the differential operations in Eq. (11), Lamb’s general solution in spherical coordinates $\mathbf{u} = u_r \mathbf{e}_r + u_\theta \mathbf{e}_\theta + u_\phi \mathbf{e}_\phi$ takes the form

$$u_r = \sum_{n=1}^{\infty} \sum_{m=0}^n \frac{(n+1)P_n^m}{2(2n-1)\eta r^{n+2}} \left\{ \left[A_{mn}r^2 - 2B_{mn}(2n-1)\eta \right] \cos m\phi + \left[\tilde{A}_{mn}r^2 - 2\tilde{B}_{mn}(2n-1)\eta \right] \sin m\phi \right\}, \tag{15}$$

$$u_\theta = \sum_{n=1}^{\infty} \sum_{m=0}^n \frac{1}{2r^n \sin \theta} \left\{ \sin^2 \theta P_n^{m'} \left[\frac{n-2}{n(2n-1)\eta} (A_{mn} \cos m\phi + \tilde{A}_{mn} \sin m\phi) - \frac{2}{r^2} (B_{mn} \cos m\phi + \tilde{B}_{mn} \sin m\phi) \right] + \frac{2m}{r} P_n^m (\tilde{C}_{mn} \cos m\phi - C_{mn} \sin m\phi) \right\}, \tag{16}$$

$$u_\phi = \sum_{n=1}^{\infty} \sum_{m=0}^n \frac{1}{2r^n \sin \theta} \left\{ m P_n^m \left[\frac{n-2}{n(2n-1)\eta} P_n^m (-\tilde{A}_{mn} \cos m\phi + A_{mn} \sin m\phi) - \frac{2}{r^2} (-\tilde{B}_{mn} \cos m\phi + B_{mn} \sin m\phi) \right] + \frac{2}{r} \sin^2 \theta P_n^{m'} (C_{mn} \cos m\phi + \tilde{C}_{mn} \sin m\phi) \right\}. \tag{17}$$

Here we have employed a recursion expression of associated Legendre polynomials,

$$(n+1)\mu P_n^m - (1+n-m)P_{n+1}^m = (1-\mu^2)P_n^{m'}, \tag{18}$$

to simplify the equations [59,60] (the primes represent differentiation with respect to the variable μ).

From the radial velocity component, Eq. (15), the requirement of purely tangential deformation leads to the relations

$$A_{mn} = \frac{2(2n-1)\eta}{a^2} B_{mn}, \quad \tilde{A}_{mn} = \frac{2(2n-1)\eta}{a^2} \tilde{B}_{mn}. \tag{19}$$

Enforcing the conditions in Eq. (19), the general flow field due to purely tangential squirring motion becomes

$$u_r = \sum_{n=1}^{\infty} \sum_{m=0}^n \frac{(n+1)P_n^m}{r^{n+2}} \left(\frac{r^2}{a^2} - 1 \right) \left[B_{mn} \cos m\phi + \tilde{B}_{mn} \sin m\phi \right], \tag{20}$$

$$u_\theta = \sum_{n=1}^{\infty} \sum_{m=0}^n \left[\sin \theta P_n^{m'} \left(\frac{n-2}{na^2 r^n} - \frac{1}{r^{n+2}} \right) (B_{mn} \cos m\phi + \tilde{B}_{mn} \sin m\phi) + \frac{m P_n^m}{r^{n+1} \sin \theta} (\tilde{C}_{mn} \cos m\phi - C_{mn} \sin m\phi) \right], \quad (21)$$

$$u_\phi = \sum_{n=1}^{\infty} \sum_{m=0}^n \left[\frac{\sin \theta P_n^{m'}}{r^{n+1}} (C_{mn} \cos m\phi + \tilde{C}_{mn} \sin m\phi) - \frac{m P_n^m}{\sin \theta} \left(\frac{n-2}{na^2 r^n} - \frac{1}{r^{n+2}} \right) (\tilde{B}_{mn} \cos m\phi - B_{mn} \sin m\phi) \right]. \quad (22)$$

To reiterate, the preceding flow fields decay at infinity in the laboratory frame and correspond to purely tangential velocities at the body surface; the case with radial velocities is detailed in Appendices B and C.

Note that for simplicity in this paper we consider a neutrally buoyant squirmer, where the buoyancy force from the fluid balances the gravitational force on the squirmer. Hence, there is no net force or torque acting on the fluid (the force- and torque-free conditions). Should there be a density offset between the squirmer and the fluid, it would result in a net force [61] and thus would add a Stokeslet component (Appendix A.1) to the flow field around the squirmer, which can be superimposed on the results of the current work.

3 Axisymmetric squirming motion

In this section, we use Lamb's general solution to reproduce the axisymmetric results first derived by Lighthill [40] and Blake [41]. The analysis also identifies new axisymmetric modes. With the general solution, Eqs. (21)–(22), the axisymmetric flow field ($m = 0$) reduces to

$$\mathbf{u}(r, \theta, \phi) = \sum_{n=1}^{\infty} \frac{(n+1)P_n}{r^{n+2}} \left(\frac{r^2}{a^2} - 1 \right) B_{0n} \mathbf{e}_r + \sum_{n=1}^{\infty} \sin \theta P_n' \left(\frac{n-2}{na^2 r^n} - \frac{1}{r^{n+2}} \right) B_{0n} \mathbf{e}_\theta + \sum_{n=1}^{\infty} \frac{\sin \theta P_n^{m'}}{r^{n+1}} C_{0n} \mathbf{e}_\phi \quad (23)$$

for purely tangential squirring motion, where we denote by $P_n(\mu) = P_n^0(\mu)$ the Legendre polynomials of degree n . The surface velocities on the sphere have the form

$$\mathbf{u}(a, \theta, \phi) = \sum_{n=1}^{\infty} -\frac{2 \sin \theta P_n'}{a^{n+2n}} B_{0n} \mathbf{e}_\theta + \sum_{n=1}^{\infty} \frac{\sin \theta P_n'}{a^{n+1}} C_{0n} \mathbf{e}_\phi. \quad (24)$$

Upon setting $C_{0n} = 0$ and using a simple rescaling

$$B_{0n} = -\frac{a^{n+2}}{n+1} B_n, \quad (25)$$

the preceding surface velocities reduce to the form used in Lighthill [40] and Blake [41], where B_n are the coefficients used in their work.

Here we have identified new axisymmetric modes, denoted C_{0n} , acting in the azimuthal direction ϕ (right-hand side of Eq. (24)) and the corresponding flow fields (last sum in Eq. (23)), which were not accounted for in previous works. While Stone and Samuel [53] and Drescher et al. [54] employed the reciprocal theorem to discuss the swimming kinematics of a squirmer subject to arbitrary squirring profiles, the current results complete the analysis of axisymmetric squirring motion by providing the whole flow field. The physical interpretation of these new axisymmetric modes is discussed subsequently in Sect. 3.2.

3.1 Swimming of an axisymmetric squirmer

When studying the swimming of a squirmer, it is best to think about the problem in two separate steps. In the first step, we consider the preceding solution, Eq. (23), with boundary conditions from Eq. (24), so that the squirmer is fixed in space (by an external force) and not allowed to move. This is sometimes referred to in the literature as the pumping problem. In the second step, we allow the squirmer to move freely and compute the induced translational (\mathbf{U}) and rotational ($\mathbf{\Omega}$) velocities, given the boundary actuation in the pumping problem, Eq. (24). This allows the separation of the surface velocities due to the boundary actuation of the squirmer from the contribution due to the induced translation and rotation. To obtain the overall flow field, \mathbf{v} , of a swimming squirmer, we superimpose the solution of the pumping problem, \mathbf{u} , and the flow fields due to the induced translation, \mathbf{u}_T , and rotation, \mathbf{u}_R , and thus write

$$\mathbf{v} = \mathbf{u} + \mathbf{u}_T + \mathbf{u}_R. \tag{26}$$

This first step (computing \mathbf{u}) was accomplished in Eq. (23). We now determine the unknown swimming kinematics, $\{\mathbf{U}, \mathbf{\Omega}\}$, when the squirmer is free to move. This involves computing all the forces and torques acting on the swimming squirmer: the fluid force, \mathbf{F}_p , and torque, \mathbf{T}_p , due to the boundary actuation in the pumping problem, and the drag, \mathbf{F}_s , and torque, \mathbf{T}_s , due to the induced translation and rotation of the squirmer. We then enforce the overall force-free and torque-free conditions in swimming problems of Stokes flows as

$$\mathbf{F}_p + \mathbf{F}_s = \mathbf{0}, \tag{27}$$

$$\mathbf{T}_p + \mathbf{T}_s = \mathbf{0}. \tag{28}$$

The drag and torque due to the translation and rotation of a spherical squirmer are simply $\mathbf{F}_s = -6\pi\eta a\mathbf{U}$ and $\mathbf{T}_s = -8\pi\eta a^3\mathbf{\Omega}$, respectively. For the contributions from the pumping problem, the net force and torque due to the boundary actuation can be conveniently computed in Lamb’s general solution as $\mathbf{F}_p = -4\pi\nabla(r^3 p_{-2})$ and $\mathbf{T}_p = -8\pi\eta\nabla(r^3 \chi_{-2})$, respectively [57,58]. The force and torque balances, Eqs. (27) and (28), therefore become

$$-4\pi\nabla(r^3 p_{-2}) - 6\pi\eta a\mathbf{U} = \mathbf{0}, \tag{29}$$

$$-8\pi\eta\nabla(r^3 \chi_{-2}) - 8\pi\eta a^3\mathbf{\Omega} = \mathbf{0}. \tag{30}$$

The solutions for p_{-2} and χ_{-2} are given by Eqs. (12) and (14), respectively, and we thus obtain the swimming kinematics

$$\mathbf{U} = -\frac{2}{3\eta a}\nabla(r P_1) A_{01} = -\frac{4B_{01}}{3a^3}\mathbf{e}_z, \tag{31}$$

$$\mathbf{\Omega} = -\frac{\nabla(r P_1)}{a^3} C_{01} = -\frac{C_{01}}{a^3}\mathbf{e}_z, \tag{32}$$

where we have used Eq. (19). Note that the propulsion and rotational velocities may also be obtained using a reciprocal theorem approach [53], as discussed in Sect. 4.2. The translational swimming velocity agrees with that given by Lighthill [40] and Blake [41] provided the rescaling from Eq. (25) is used, giving $\mathbf{U} = 2B_1/3\mathbf{e}_z$.

For an axisymmetric squirmer, propulsion and rotation can only occur in the same direction (here, the z -direction), and hence the squirmer can only follow a straight swimming trajectory. Also notice that among all the modes in the squirring profile, Eq. (24), just one mode, mode B_{01} , contributes to propulsion. Similarly, among all the new azimuthal modes in the boundary condition, only mode C_{01} contributes to the rotation of the squirmer.

Finally, by superimposing the solution of the pumping problem, Eq. (26), and the flow fields due to the swimming kinematics, Eqs. (31) and (32), we obtain the overall flow field of an axisymmetric swimming squirmer, $\mathbf{v} = v_r\mathbf{e}_r + v_\theta\mathbf{e}_\theta + v_\phi\mathbf{e}_\phi$, in the laboratory frame as

$$v_r = -\frac{4\cos\theta}{3r^3}B_{01} + \sum_{n=2}^{\infty} \frac{(n+1)P_n}{r^{n+2}} \left(\frac{r^2}{a^2} - 1\right) B_{0n}, \tag{33}$$

$$v_\theta = -\frac{2\sin\theta}{3r^3}B_{01} + \sum_{n=2}^{\infty} \sin\theta P'_n \left(\frac{n-2}{na^2r^n} - \frac{1}{r^{n+2}}\right) B_{0n}, \tag{34}$$

$$v_\phi = \sum_{n=2}^{\infty} \frac{\sin \theta P'_n}{r^{n+1}} C_{0n}. \quad (35)$$

Note that throughout the paper we will refer to the flow fields in the pumping and swimming problems as \mathbf{u} and \mathbf{v} , respectively.

3.2 Axisymmetric flow structure

In this section, we identify the flow structure generated by a swimming squirmer as due to a superposition of flow singularities. This allows a physical interpretation of the flows caused by different modes of ciliary action in terms of combinations of point forces and torques and their spatial derivatives [42]. Such an understanding is useful for constructing approximations for swimmers in theoretical modeling and computer simulations, where one can retain only modes relevant to the aspects of physics of interest. For instance, in the axisymmetric case, it is common to retain only the mode contributing to swimming (the source dipole mode) and the mode due to two point forces (Stokes dipoles) [42, 44–46], where the arrangement of the two-point forces (the sign of the Stokes dipole) can represent different types of swimmers (pushers vs. pullers; see Sect. 1). In what follows, we first revisit the known correspondences between the flow field around an axisymmetric squirmer and different flow singularities. We then proceed to discuss the new axisymmetric modes and the interpretation of their corresponding flow singularities.

3.2.1 The B_{01} mode

The primary fundamental singularity in Stokes flows is the flow due to a point force $f\boldsymbol{\alpha}\delta(\mathbf{r})$ of magnitude f and direction $\boldsymbol{\alpha}$ at the origin, where $\delta(\mathbf{r})$ is the Dirac delta function. The solution is given by $\mathbf{u} = f\mathbf{G}(\boldsymbol{\alpha})/(8\pi\eta)$, where

$$\mathbf{G}(\boldsymbol{\alpha}) = \frac{1}{r} [\boldsymbol{\alpha} + (\boldsymbol{\alpha} \cdot \mathbf{e}_r)\mathbf{e}_r], \quad (36)$$

and is called a Stokeslet. That flow is long-ranged and decays as $1/r$. A Stokeslet acting in the z -direction has the explicit form in spherical coordinates

$$\mathbf{G}(\mathbf{e}_z) = \frac{1}{r} [2 \cos \theta \mathbf{e}_r - \sin \theta \mathbf{e}_\theta]. \quad (37)$$

In the pumping problem, Eq. (23), we can then identify that the B_{01} mode,

$$\mathbf{u}_{B_{01}} = \left(\frac{2P_1}{a^2r} - \frac{2P_1}{r^3} \right) B_{01} \mathbf{e}_r + \left(-\frac{\sin \theta P'_1}{a^2r} - \frac{\sin \theta P'_1}{r^3} \right) B_{01} \mathbf{e}_\theta \quad (38)$$

$$= \frac{B_{01}}{a^2r} (2 \cos \theta \mathbf{e}_r - \sin \theta \mathbf{e}_\theta) - \frac{B_{01}}{r^3} (2 \cos \theta \mathbf{e}_r + \sin \theta \mathbf{e}_\theta), \quad (39)$$

contains a Stokeslet in the z -direction (Eq. 37). The other component, decaying faster as $1/r^3$, corresponds to a source dipole singularity, also in the z -direction, which we discuss subsequently (Eq. 53).

To obtain the overall flow field, \mathbf{v} , surrounding a swimming squirmer, Eq. (26), the solution to the pumping problem, \mathbf{u} , needs to be superimposed by that due to a translating sphere at a velocity $-4B_{01}/3a^3$, Eq. (31), leading to

$$\mathbf{u}_T = -\frac{B_{01}}{a^2r} (2 \cos \theta \mathbf{e}_r - \sin \theta \mathbf{e}_\theta) + \frac{B_{01}}{3r^3} (2 \cos \theta \mathbf{e}_r + \sin \theta \mathbf{e}_\theta), \quad (40)$$

which also contains a Stokeslet and a source dipole. Unsurprisingly, the Stokeslet components cancel each other exactly and satisfy the overall force-free condition of a free swimming squirmer. Therefore, a Stokeslet component does not appear in the swimming flow field from Eqs. (33)–(35). Notice, however, that the cancellation of the source dipole components is incomplete, leaving a residual source dipole in the swimming flow field as

$$\mathbf{v}_{B_{01}} = -\frac{2B_{01}}{3r^3} (2 \cos \theta \mathbf{e}_r + \sin \theta \mathbf{e}_\theta). \quad (41)$$

3.2.2 The B_{02} and C_{01} modes

Analyzing the structure of flow around a swimming squirmer from Eqs. (33)–(35), we see that the slowest decaying flow field ($\sim 1/r^2$) is contained in the B_{02} mode as

$$\mathbf{v}_{B_{02}} = \frac{3P_2}{r^4} \left(\frac{r^2}{a^2} - 1 \right) B_{02} \mathbf{e}_r - \frac{\sin \theta P_2'}{r^4} B_{02} \mathbf{e}_\theta \tag{42}$$

$$= \frac{3B_{02}}{4a^2r^2} (1 + 3 \cos 2\theta) \mathbf{e}_r - \frac{3B_{02}}{4r^4} [(1 + 3 \cos 2\theta) \mathbf{e}_r + 2 \sin 2\theta \mathbf{e}_\theta]. \tag{43}$$

The part decaying as $1/r^2$ can be interpreted as the contribution of a Stokes dipole, which is a higher-order singularity of Stokes flows, and obtained by taking a derivative of a Stokeslet (directed in the $\boldsymbol{\alpha}$ -direction) along the direction $\boldsymbol{\beta}$,

$$\mathbf{G}_D(\boldsymbol{\beta}, \boldsymbol{\alpha}) = \boldsymbol{\beta} \cdot \nabla \mathbf{G}(\boldsymbol{\alpha}) = \frac{(\boldsymbol{\beta} \times \boldsymbol{\alpha}) \mathbf{e}_r}{r^2} - \frac{(\boldsymbol{\beta} \cdot \boldsymbol{\alpha}) \mathbf{e}_r - 3(\boldsymbol{\alpha} \cdot \mathbf{e}_r)(\boldsymbol{\beta} \cdot \mathbf{e}_r) \mathbf{e}_r}{r^2}. \tag{44}$$

The symmetric part of a Stokes dipole is termed a stresslet, first defined by Batchelor [62], and given by

$$\mathbf{S}(\boldsymbol{\beta}, \boldsymbol{\alpha}) = -\frac{(\boldsymbol{\beta} \cdot \boldsymbol{\alpha}) \mathbf{e}_r - 3(\boldsymbol{\alpha} \cdot \mathbf{e}_r)(\boldsymbol{\beta} \cdot \mathbf{e}_r) \mathbf{e}_r}{r^2}, \tag{45}$$

which physically represents the straining motion of the fluid. The antisymmetric part is termed a rotlet,

$$\mathbf{R}(\boldsymbol{\zeta}) = \frac{\boldsymbol{\zeta} \times \mathbf{e}_r}{r^2}, \tag{46}$$

where $\boldsymbol{\zeta} = \boldsymbol{\beta} \times \boldsymbol{\alpha}$ represents the strength (magnitude and direction) of the flow due to a singular point torque. The Stokes dipole with $\boldsymbol{\alpha} = \boldsymbol{\beta} = \mathbf{e}_z$ corresponds to only a stresslet

$$\mathbf{G}_D(\mathbf{e}_z, \mathbf{e}_z) = \mathbf{S}(\mathbf{e}_z, \mathbf{e}_z) = \frac{1 + 3 \cos 2\theta}{r^2} \mathbf{e}_r. \tag{47}$$

In the B_{02} mode of the flow field, Eq. (42), we can readily identify a Stokes dipole (stresslet) (see Appendices A.2 and A.3), while the other part decaying as $1/r^4$ corresponds to a source quadrupole, a higher-order singularity.

The first azimuthal mode in the pumping problem, Eq. (23), is given by the C_{01} mode,

$$\mathbf{u}_{C_{01}} = \frac{\sin \theta P_1'}{r^2} C_{01} \mathbf{e}_\phi = \frac{\sin \theta}{r^2} C_{01} \mathbf{e}_\phi, \tag{48}$$

and represents a rotlet in the z -direction, $\mathbf{R}(\mathbf{e}_z) = \sin \theta / r^2 \mathbf{e}_\phi$. Similar to the translation case, the pumping problem solution, \mathbf{u} , is superimposed by the flow field due to the induced rotation at the rate $-C_{01}/a^3$ (Eq. 32)

$$\mathbf{u}_R = -\frac{\sin \theta}{r^2} C_{01}, \tag{49}$$

leading to the total flow field surrounding a swimming squirmer, \mathbf{v} (Eq. 26). Again, unsurprisingly, the rotlet components exerting torques on the fluid cancel out completely, thereby satisfying the overall torque-free condition. The C_{01} mode is hence absent from the resulting swimming flow field, Eqs. (33)–(35), leaving no trace of the rotational motion of the squirmer. The important difference between rotation and translation is that the rotational mode is due to velocities that are all in the direction of the rotation, so a complete cancellation of the flow field satisfying the torque-free condition is possible by simply rotating in the opposite direction at the same rate. In contrast, for translational swimming, such exact cancellation is not possible because the surface velocity has a distribution of directions all along the sphere relative to its swimming direction. In other words, one can construct the ultimate stealth rotating sphere using purely tangential modes but not a similarly stealth translating sphere.

In summary, the B_{02} and C_{01} modes together contain the representation of a Stokes dipole (stresslet plus rotlet) with the direction and gradient taken both in the z -direction ($\boldsymbol{\alpha} = \boldsymbol{\beta} = \mathbf{e}_z$).

3.2.3 The B_{03} and C_{02} modes

Higher-order flow singularities can be obtained by repeatedly taking derivatives of the lower-order singularities. Full vector expressions of these singularities can be found in the literature Spagnolie and Lauga [67]. For example, a Stokes quadrupole can be obtained by taking a derivative of a Stokes dipole, $\mathbf{G}_D(\boldsymbol{\beta}, \boldsymbol{\alpha})$, along the direction $\boldsymbol{\gamma}$, leading to

$$\begin{aligned} \mathbf{G}_Q(\boldsymbol{\gamma}, \boldsymbol{\beta}, \boldsymbol{\alpha}) &= \boldsymbol{\gamma} \cdot \nabla \mathbf{G}(\boldsymbol{\beta}, \boldsymbol{\alpha}) \\ &= \frac{1}{r^3} \left\{ (\boldsymbol{\beta} \cdot \boldsymbol{\alpha}) \boldsymbol{\gamma} + (\boldsymbol{\gamma} \cdot \boldsymbol{\alpha}) \boldsymbol{\beta} - (\boldsymbol{\gamma} \cdot \boldsymbol{\beta}) \boldsymbol{\alpha} + 15(\boldsymbol{\gamma} \cdot \mathbf{e}_r)(\boldsymbol{\beta} \cdot \mathbf{e}_r)(\boldsymbol{\alpha} \cdot \mathbf{e}_r) \mathbf{e}_r \right. \\ &\quad \left. - 3 [(\boldsymbol{\beta} \cdot \boldsymbol{\alpha})(\boldsymbol{\gamma} \cdot \mathbf{e}_r) + (\boldsymbol{\gamma} \cdot \boldsymbol{\alpha})(\boldsymbol{\beta} \cdot \mathbf{e}_r) + (\boldsymbol{\gamma} \cdot \boldsymbol{\beta})(\boldsymbol{\alpha} \cdot \mathbf{e}_r)] \mathbf{e}_r \right. \\ &\quad \left. - 3 [(\boldsymbol{\gamma} \cdot \mathbf{e}_r)(\boldsymbol{\alpha} \cdot \mathbf{e}_r) \boldsymbol{\gamma} + (\boldsymbol{\gamma} \cdot \mathbf{e}_r)(\boldsymbol{\alpha} \cdot \mathbf{e}_r) \boldsymbol{\beta} - (\boldsymbol{\gamma} \cdot \mathbf{e}_r)(\boldsymbol{\beta} \cdot \mathbf{e}_r) \boldsymbol{\alpha}] \right\}. \end{aligned} \quad (50)$$

The flow field due to such a Stokes quadrupole decays as $1/r^3$. In particular, a Stokes quadrupole with $\boldsymbol{\alpha} = \boldsymbol{\beta} = \boldsymbol{\gamma} = \mathbf{e}_z$ takes the simple form

$$\mathbf{G}_Q(\mathbf{e}_z, \mathbf{e}_z, \mathbf{e}_z) = \frac{1}{r^3} \left[(\cos \theta + 3 \cos 3\theta) \mathbf{e}_r + \frac{1}{4} (3 \sin 3\theta - \sin \theta) \mathbf{e}_\theta \right], \quad (51)$$

which is useful in interpreting the B_{03} mode in Lamb's solution, as we will see below.

Several components of the Stokes quadrupole have particularly clear physical meanings, such as the potential (source) dipole

$$\mathbf{P}_D(\boldsymbol{\alpha}) = \frac{1}{r^3} [-\boldsymbol{\alpha} + 3(\boldsymbol{\alpha} \cdot \mathbf{e}_r) \mathbf{e}_r], \quad (52)$$

where $\boldsymbol{\alpha}$ denotes its direction. A potential dipole in the z -direction is given by

$$\mathbf{P}_D(\mathbf{e}_z) = \frac{1}{r^3} [2 \cos \theta \mathbf{e}_r + \sin \theta \mathbf{e}_\theta], \quad (53)$$

which is the residual component of the B_{01} mode in the overall flow field of a swimming squirmer (see Eq. (41) or Eqs. (33)–(35)). This potential dipole component contained in the B_{01} mode, together with the part decaying as $1/r^3$ in the B_{03} mode and given by

$$\begin{aligned} \mathbf{v}_{B_{03}} &= \frac{B_{03}}{2a^2 r^3} \left[(3 \cos \theta + 5 \cos 3\theta) \mathbf{e}_r + \frac{1}{4} (\sin \theta + 5 \sin 3\theta) \mathbf{e}_\theta \right] \\ &\quad - \frac{B_{03}}{2r^5} \left[(3 \cos \theta + 5 \cos 3\theta) \mathbf{e}_r + \frac{3}{4} (\sin \theta + 5 \sin 3\theta) \mathbf{e}_\theta \right], \end{aligned} \quad (54)$$

contains the representation of the Stokes quadrupole, $\mathbf{G}_Q(\mathbf{e}_z, \mathbf{e}_z, \mathbf{e}_z)$, expressed in Eq. (51). The other component decaying as $1/r^5$ in the B_{03} mode corresponds to a source octupole.

The first azimuthal component appearing in the flow field around a swimming squirmer is given by the C_{02} mode

$$\mathbf{v}_{C_{02}} = \frac{3 \sin 2\theta}{2r^3} C_{02} \mathbf{e}_\phi, \quad (55)$$

which represents another well-known component of the Stokes quadrupole, called a rotlet dipole. A rotlet dipole can be obtained by taking a derivative along the $\boldsymbol{\gamma}$ direction of a rotlet with the direction $\boldsymbol{\zeta} = \boldsymbol{\beta} \times \boldsymbol{\alpha}$

$$\mathbf{R}_D(\boldsymbol{\gamma}, \boldsymbol{\zeta}) = \boldsymbol{\gamma} \cdot \nabla \mathbf{R}(\boldsymbol{\zeta}) = \frac{1}{r^3} \left[\boldsymbol{\gamma} \times \boldsymbol{\zeta} + \frac{3(\boldsymbol{\gamma} \cdot \mathbf{e}_r)(\boldsymbol{\zeta} \times \mathbf{e}_r)}{r^3} \right]. \quad (56)$$

In particular, a rotlet dipole with $\boldsymbol{\gamma} = \boldsymbol{\zeta} = \mathbf{e}_z$ takes the simple form $\mathbf{R}_D(\mathbf{e}_z, \mathbf{e}_z) = 3 \sin 2\theta / 2r^3 \mathbf{e}_\phi$. This corresponds to the C_{02} mode in Lamb's general solution, Eq. (55), and provides the leading-order mode in the azimuthal direction. In Fig. 3, we plot the slowest decaying flow field, given by the B_{02} mode with $B_{02} = 1$ (a stresslet in the far field, Fig. 3a; a pusher, see Sect. 1), as well as the slowest decaying flow in the azimuthal direction, given by the C_{02} mode with $C_{02} = 1$ (a rotlet dipole, Fig. 3b).

To summarize, the B_{01} and B_{03} modes contain physically the Stokes quadrupole, $\mathbf{G}_Q(\mathbf{e}_z, \mathbf{e}_z, \mathbf{e}_z)$; the C_{02} mode corresponds to a rotlet dipole, $\mathbf{R}_D(\mathbf{e}_z, \mathbf{e}_z) = 3 \sin 2\theta / 2r^3 \mathbf{e}_\phi$, which is part of a Stokes quadrupole that is different than $\mathbf{G}_Q(\mathbf{e}_z, \mathbf{e}_z, \mathbf{e}_z)$ (see also Sect. 4.3 for further details).

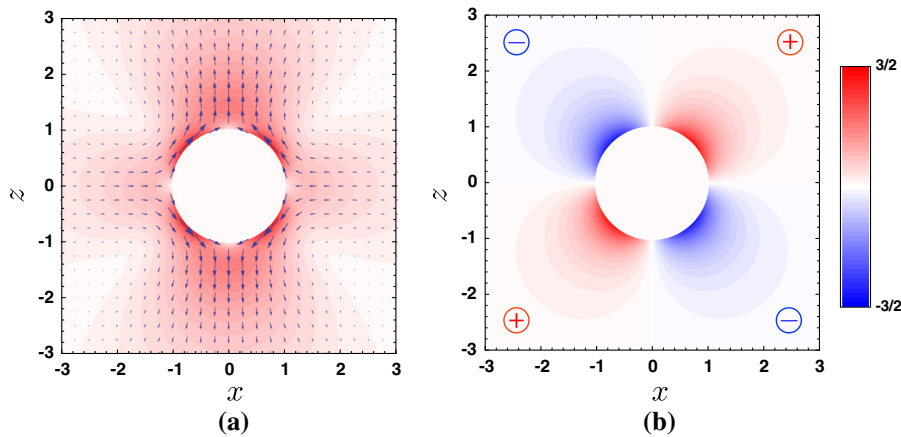


Fig. 3 Flow fields due to axisymmetric squirring motion of sphere of radius $a = 1$. **a** Flow field due to B_{02} mode with $B_{02} = 1$, $\mathbf{v}_{B_{02}} = 3(1 + 3 \cos 2\theta)B_{02}/4a^2r^2\mathbf{e}_r - 3[(1 + 3 \cos 2\theta)\mathbf{e}_r + 2 \sin 2\theta\mathbf{e}_\theta]B_{02}/4r^4$, which is a source quadrupole in the near field and a stresslet in the far field (a pusher, see Sect. 1). The color density represents the flow speed. **b** Flow field due to C_{02} mode with $C_{02} = 1$, $\mathbf{v}_{C_{02}} = 3 \sin 2\theta C_{02}/2r^3\mathbf{e}_\phi$ (a rotlet dipole), with all the velocities in the azimuthal (ϕ) direction, i.e., perpendicular to the page. The color density represents the speed, with red and blue denoting positive “+” (into page) and negative “-” (out of page) velocities in different quadrants

4 Nonaxisymmetric squirring motion

We now generalize the results for axisymmetric swimming to the nonaxisymmetric case using Eqs. (21)–(22). The velocities on the surface of the sphere for this general case are given by

$$u_r|_{r=a} = 0, \tag{57}$$

$$u_\theta|_{r=a} = \sum_{n=1}^{\infty} \sum_{m=0}^n \left[-\frac{2 \sin \theta P_n^{m'}}{na^{n+2}} \left(B_{mn} \cos m\phi + \tilde{B}_{mn} \sin m\phi \right) + \frac{m P_n^m}{a^{n+1} \sin \theta} \left(\tilde{C}_{mn} \cos m\phi - C_{mn} \sin m\phi \right) \right], \tag{58}$$

$$u_\phi|_{r=a} = \sum_{n=1}^{\infty} \sum_{m=0}^n \left[\frac{\sin \theta P_n^{m'}}{a^{n+1}} \left(C_{mn} \cos m\phi + \tilde{C}_{mn} \sin m\phi \right) + \frac{2m P_n^m}{na^{n+2} \sin \theta} \left(\tilde{B}_{mn} \cos m\phi - B_{mn} \sin m\phi \right) \right]. \tag{59}$$

Recall that the more general analysis, which includes nonzero radial surface velocities, is given in Appendices B and C, and we focus in what follows on the swimming problem of a nonaxisymmetric squirmer with purely tangential squirring profiles.

4.1 Swimming of a nonaxisymmetric squirmer

We follow closely the analysis presented in the axisymmetric case (Sect. 3) to investigate the situation where the surface motion is nonaxisymmetric. As discussed in Sect. 3.1, we consider the swimming problem as a superposition of a pumping problem with the boundary actuation in Eqs. (57)–(59) and the flow field due to the induced translation and rotation of the squirmer (given in Eq. (26)). Applying the force and torque balances in this nonaxisymmetric case, the results from Eqs. (29) and (30) continue to hold, but with solutions for p_{-2} and χ_{-2} , which are more involved, resulting in

$$\mathbf{U} = -\frac{2}{3\eta a} \nabla \left[r \left(P_1 A_{01} + P_1^1 \cos \phi A_{11} + P_1^1 \sin \phi \tilde{A}_{11} \right) \right] = \frac{4}{3a^3} \left(B_{11}\mathbf{e}_x + \tilde{B}_{11}\mathbf{e}_y - B_{01}\mathbf{e}_z \right), \tag{60}$$

$$\mathbf{\Omega} = -\frac{1}{a^3} \nabla \left[r \left(P_1 C_{01} + P_1^1 \cos \phi C_{11} + P_1^1 \sin \phi \tilde{C}_{11} \right) \right] = \frac{1}{a^3} \left(C_{11}\mathbf{e}_x + \tilde{C}_{11}\mathbf{e}_y - C_{01}\mathbf{e}_z \right). \tag{61}$$

For an axisymmetric squirmer, only the B_{01} and C_{01} modes contribute to propulsion and rotation, respectively. In contrast, for a general nonaxisymmetric squirmer, Eqs. (60) and (61) identify all the modes contributing to its three-dimensional locomotion. Specifically, three modes, B_{11} , \tilde{B}_{11} , and B_{01} , contribute to the translational swimming

in the x -, y -, and z -directions, respectively; similarly, three modes, C_{11} , \tilde{C}_{11} , and C_{01} , lead to rotation in the x -, y -, and z -directions, respectively. By superimposing the flow fields due to the induced translation and rotation according to the velocities determined, Eqs. (60) and (61), with the solution to the nonaxisymmetric pumping problem, Eqs. (21)–(22), we obtain the flow field around a nonaxisymmetric swimming squirmer as

$$v_r = \frac{4}{3r^3} \left(B_{11} \sin \theta \cos \phi + \tilde{B}_{11} \sin \theta \sin \phi - B_{01} \cos \theta \right) + \sum_{n=2}^{\infty} \sum_{m=0}^n \frac{(n+1)P_n^m}{r^{n+2}} \left(\frac{r^2}{a^2} - 1 \right) \left[B_{mn} \cos m\phi + \tilde{B}_{mn} \sin m\phi \right], \quad (62)$$

$$v_\theta = -\frac{2}{3r^3} \left(B_{11} \cos \theta \cos \phi + \tilde{B}_{11} \cos \theta \sin \phi + B_{01} \sin \theta \right) + \sum_{n=2}^{\infty} \sum_{m=0}^n \left[\sin \theta P_n^{m'} \left(\frac{n-2}{na^2r^n} - \frac{1}{r^{n+2}} \right) \left(B_{mn} \cos m\phi + \tilde{B}_{mn} \sin m\phi \right) + \frac{mP_n^m}{r^{n+1} \sin \theta} \left(\tilde{C}_{mn} \cos m\phi - C_{mn} \sin m\phi \right) \right], \quad (63)$$

$$v_\phi = \frac{2}{3r^3} \left(B_{11} \sin \phi - \tilde{B}_{11} \cos \phi \right) + \sum_{n=2}^{\infty} \sum_{m=0}^n \left[\frac{\sin \theta P_n^{m'}}{r^{n+1}} \left(C_{mn} \cos m\phi + \tilde{C}_{mn} \sin m\phi \right) - \frac{mP_n^m}{\sin \theta} \left(\frac{n-2}{na^2r^n} - \frac{1}{r^{n+2}} \right) \left(\tilde{B}_{mn} \cos m\phi - B_{mn} \sin m\phi \right) \right]. \quad (64)$$

The flow reduces to Eqs. (33)–(35) in the axisymmetric case ($m = 0$). The physical meaning of the new nonaxisymmetric terms ($m \neq 0$) is interpreted in Sect. 4.3.

4.2 Swimming kinematics by integral theorems

The swimming kinematics of a squirmer can also be arrived using the reciprocal theorem approach taken by Stone and Samuel [53] without having to solve for the whole flow field. The theorem relates the swimming velocity to the surface distortion, $\mathbf{u}|_{r=a}$, via a surface integral on the sphere S ,

$$\mathbf{U} = -\frac{1}{4\pi a^2} \int_S \mathbf{u}|_{r=a} dS, \quad (65)$$

which in spherical coordinates reads

$$\mathbf{U} = -\frac{1}{4\pi} \int_0^{2\pi} \int_{-1}^1 (u_\theta \mathbf{e}_\theta + u_\phi \mathbf{e}_\phi)_{r=a} d\mu d\phi. \quad (66)$$

By transforming the basis vectors in spherical coordinates to those in Cartesian coordinates, the integral simplifies due to the orthogonality of sinusoidal functions in the azimuthal angle ϕ , and we obtain

$$\begin{aligned} \mathbf{U} = & -\frac{1}{4} \sum_{n=1}^{\infty} \left\{ \frac{\tilde{C}_{1n}}{a^{n+1}} \int_{-1}^1 \left(P_1^{1'} P_n^1 + P_1^1 P_n^{1'} \right) d\mu - \frac{2B_{1n}}{na^{n+2}} \int_{-1}^1 \left[(1-\mu^2) P_1^{1'} P_n^{1'} + \frac{P_1^1 P_n^1}{1-\mu^2} \right] d\mu \right\} \mathbf{e}_x \\ & -\frac{1}{4} \sum_{n=1}^{\infty} \left\{ \frac{C_{1n}}{a^{n+1}} \int_{-1}^1 \left(P_1^{1'} P_n^1 + P_1^1 P_n^{1'} \right) d\mu - \frac{2\tilde{B}_{1n}}{na^{n+2}} \int_{-1}^1 \left[(1-\mu^2) P_1^{1'} P_n^{1'} + \frac{P_1^1 P_n^1}{1-\mu^2} \right] d\mu \right\} \mathbf{e}_y \\ & -\frac{1}{2} \sum_{n=1}^{\infty} \left[\frac{2B_{0n}}{a^{n+2}n} \int_{-1}^1 (1-\mu^2) P_1^{1'} P_n^{1'} d\mu \right] \mathbf{e}_z. \end{aligned} \quad (67)$$

The integrals associated with C_{1n} and \tilde{C}_{1n} vanish upon integration by parts. The remaining integrals can be evaluated using a general expression derived below (Eq. 78) in the special cases of $m = 0$ and 1. We then obtain results identical to those given by Lamb’s solution, Eq. (60). Similarly, one can employ the reciprocal theorem to derive the rotational velocity, [53]

$$\boldsymbol{\Omega} = -\frac{3}{8\pi a^3} \int_S \mathbf{n} \times \mathbf{u}|_{r=a} dS, \tag{68}$$

and obtain the same result as earlier (Eq. 61). However, while the reciprocal theorem is a useful tool for determining swimming kinematics, it provides no information about the flow around the swimmer, which is a main result of our work.

4.3 Nonaxisymmetric flow structure

In the axisymmetric case, we have interpreted the flow fields due to different modes of the squirring profile as fundamental flow singularities. We extend the idea here to physically interpret the flow induced by the nonaxisymmetric terms. Note that in each of the modes discussed subsequently, the corresponding flow field is not a far-field approximation of the flow induced by the squirmer but an exact solution valid in the entire space, and it is an appropriate superposition of these modes that satisfies arbitrary boundary conditions on the spherical surface.

4.3.1 The B_{11} and \tilde{B}_{11} modes

In Sect. 3.2, we identified that part of the B_{01} mode of Lamb’s solution in the pumping problem, Eqs. (57)–(59), corresponds to a Stokeslet directed in the z -direction. One can then verify that other nonaxisymmetric modes decaying as $1/r$ in Lamb’s solution, namely B_{11} and \tilde{B}_{11} , with the flow fields

$$\begin{aligned} \mathbf{u}_{B_{11}} = & \frac{B_{11}}{a^2 r} (-2 \cos \theta \cos \phi \mathbf{e}_r - \cos \theta \cos \phi \mathbf{e}_\theta + \sin \phi \mathbf{e}_\phi) \\ & + \frac{B_{11}}{r^3} (2 \sin \theta \cos \phi \mathbf{e}_r - \cos \theta \cos \phi \mathbf{e}_\theta + \sin \phi \mathbf{e}_\phi), \end{aligned} \tag{69}$$

$$\begin{aligned} \mathbf{u}_{\tilde{B}_{11}} = & \frac{\tilde{B}_{11}}{a^2 r} (-2 \sin \theta \sin \phi \mathbf{e}_r - \cos \theta \sin \phi \mathbf{e}_\theta - \cos \phi \mathbf{e}_\phi) \\ & + \frac{\tilde{B}_{11}}{r^3} (2 \sin \theta \sin \phi \mathbf{e}_r - \cos \theta \sin \phi \mathbf{e}_\theta - \cos \phi \mathbf{e}_\phi), \end{aligned} \tag{70}$$

contain Stokeslets directed in the x - and y -directions, respectively (Appendix A.1). Similarly, the parts decaying as $1/r^3$ in the B_{11} and \tilde{B}_{11} modes correspond to potential dipoles in the x - and y -directions, respectively (Appendix A.6).

Naturally, all Stokeslet components are cancelled out exactly upon the superposition with the flow fields due to translational swimming in different directions, Eq. (60), satisfying the force-free condition and leaving only residual potential dipoles in different directions in the flow field of a nonaxisymmetric swimming squirmer, Eqs. (62)–(64).

4.3.2 The B_{m2} , \tilde{B}_{m2} , C_{11} , and \tilde{C}_{11} modes ($1 \leq m \leq 2$)

Once all the Stokeslet contributions have been removed, the slowest decaying components in the flow around a general (nonaxisymmetric) swimming squirmer, Eqs. (62)–(64), decay as $1/r^2$, which are associated with the B_{02} , B_{m2} , and \tilde{B}_{m2} modes ($1 \leq m \leq 2$). The parts decaying as $1/r^2$ in the nonaxisymmetric terms (B_{m2} and \tilde{B}_{m2}) have the same physical meaning as that in the axisymmetric B_{02} mode – these are stresslets – but they are formed by taking a gradient along various directions of a Stokeslet, itself aligned in different directions. Specifically, the B_{12} mode alone contains the stresslet $\mathbf{S}(\mathbf{e}_z, \mathbf{e}_x)$. The $\sim 1/r^2$ components in the B_{22} and B_{02} modes can be combined

to represent the stresslet $\mathbf{S}(\mathbf{e}_x, \mathbf{e}_x)$, formed by taking the gradient along \mathbf{e}_x of a Stokeslet directed also in \mathbf{e}_x . Alternatively, one can understand that a component decaying as $1/r^2$ in the B_{22} mode alone represents a stresslet formed by the superposition of $\mathbf{S}(\mathbf{e}_x, \mathbf{e}_x)$ and $-\mathbf{S}(\mathbf{e}_z, \mathbf{e}_z)$. We refer the reader to Appendix A.3 for the expressions of all stresslets in different configurations. The correspondence between stresslets with different configurations and the modes in Lamb's general solution is summarized in Table 1.

As first proposed by Batchelor [62], we can also write down a stresslet tensor in the Cartesian coordinates containing the contributions from different modes of squirmer motion, and we obtain

$$\mathbf{S} = -\frac{8\pi\eta}{a^2} \begin{pmatrix} -\frac{B_{02}}{2} + 3B_{22} & 3\tilde{B}_{22} & -\frac{3}{2}B_{12} \\ 3\tilde{B}_{22} & -\frac{B_{02}}{2} - 3B_{22} & -\frac{3}{2}\tilde{B}_{12} \\ -\frac{3}{2}B_{12} & -\frac{3}{2}\tilde{B}_{12} & B_{02} \end{pmatrix}. \quad (71)$$

That equation, allowing to determine the exact far-field nature of a generalized squirmer, is one of the important results of our paper.

In the pumping solution, Eqs. (21)–(22), the C_{02} , C_{11} , and \tilde{C}_{11} modes in Lamb's solution also decay as $1/r^2$. However, they do not contribute to the overall flow field in the swimming problem due to the torque-free condition. Similar to the C_{02} mode, the C_{11} and \tilde{C}_{11} modes represent rotlets in the x - and y -directions, respectively. Expressions of rotlets with different configurations are reproduced in Appendix A.4.

4.3.3 The B_{q3} , \tilde{B}_{q3} , C_{m2} , and \tilde{C}_{m2} modes ($1 \leq q \leq 3$ and $1 \leq m \leq 2$)

In a similar fashion, one can identify that the B_{q3} , \tilde{B}_{q3} , C_{m2} , and \tilde{C}_{m2} modes ($1 \leq q \leq 3$ and $1 \leq m \leq 2$) have the same physical meaning as their counterparts in the axisymmetric case (namely the B_{03} and C_{02} modes). Together with the parts decaying as $1/r^3$ in the B_{01} , B_{11} , and \tilde{B}_{11} modes, the six modes B_{03} , B_{q3} , \tilde{B}_{q3} , C_{02} , C_{m2} , and \tilde{C}_{m2} contain the representation of a general Stokes quadrupole with all possible geometrical configurations. Which mode corresponds to which quadrupole is summarized in Table 2.

In particular, we can identify the modes associated with better known components of the Stokes quadrupole, namely the potential dipoles and the rotlet dipoles. The flow fields associated with modes B_{11} and \tilde{B}_{11} , and decaying as $1/r^3$, correspond to potential dipoles in the x - and y -directions, respectively (Table 3 and Appendix A.6). The C_{02} , C_{m2} , and \tilde{C}_{m2} modes with the potential dipole modes (B_{01} , B_{11} and \tilde{B}_{11}) contain the representation of a general three-dimensional rotlet dipole with different configurations (Table 3 and Appendix A.7).

At this point it should be clear that the flow field generated by a swimming squirmer, Eqs. (62)–(64), may also be viewed as combinations of fundamental flow singularities. The nonaxisymmetric terms have the same physical meanings as their counterparts in the axisymmetric case (with the same value of n in Eqs. (21)–(22)), but they

Table 1 Correspondence between force dipoles (stresslets plus rotlets) and different modes of squirmer motion

Force dipole ($\sim 1/r^2$)	Contained in modes	Stresslet ($\sim 1/r^2$)	Contained in modes	Rotlet ($\sim 1/r^2$)	Contained in modes
$\mathbf{G}_D(\mathbf{e}_x, \mathbf{e}_x)$	B_{02}, B_{22}	$\mathbf{S}(\mathbf{e}_x, \mathbf{e}_x) = \mathbf{G}_D(\mathbf{e}_x, \mathbf{e}_x)$	B_{02}, B_{22}	$\mathbf{R}_D(\mathbf{e}_x)$	C_{11}
$\mathbf{G}_D(\mathbf{e}_y, \mathbf{e}_x)$	\tilde{B}_{22}, C_{01}	$\mathbf{S}(\mathbf{e}_y, \mathbf{e}_x) = \mathbf{S}(\mathbf{e}_x, \mathbf{e}_y)$	\tilde{B}_{22}	$\mathbf{R}_D(\mathbf{e}_y)$	\tilde{C}_{11}
$\mathbf{G}_D(\mathbf{e}_z, \mathbf{e}_x)$	B_{12}, \tilde{C}_{11}	$\mathbf{S}(\mathbf{e}_z, \mathbf{e}_x) = \mathbf{S}(\mathbf{e}_x, \mathbf{e}_z)$	B_{12}	$\mathbf{R}_D(\mathbf{e}_z)$	C_{01}
$\mathbf{G}_D(\mathbf{e}_x, \mathbf{e}_y)$	\tilde{B}_{22}, C_{01}	$\mathbf{S}(\mathbf{e}_y, \mathbf{e}_y) = \mathbf{G}_D(\mathbf{e}_y, \mathbf{e}_y)$	B_{02}, B_{22}		
$\mathbf{G}_D(\mathbf{e}_y, \mathbf{e}_y)$	B_{02}, B_{22}	$\mathbf{S}(\mathbf{e}_z, \mathbf{e}_y) = \mathbf{S}(\mathbf{e}_z, \mathbf{e}_y)$	\tilde{B}_{12}		
$\mathbf{G}_D(\mathbf{e}_z, \mathbf{e}_y)$	\tilde{B}_{12}, C_{11}	$\mathbf{S}(\mathbf{e}_z, \mathbf{e}_z) = \mathbf{G}_D(\mathbf{e}_z, \mathbf{e}_z)$	B_{02}		
$\mathbf{G}_D(\mathbf{e}_x, \mathbf{e}_z)$	B_{12}, \tilde{C}_{11}				
$\mathbf{G}_D(\mathbf{e}_y, \mathbf{e}_z)$	\tilde{B}_{12}, C_{11}				
$\mathbf{G}_D(\mathbf{e}_z, \mathbf{e}_z)$	B_{02}				

Table 2 Correspondence between force quadrupoles and different modes of squirring motion

Force quadrupole ($\sim 1/r^3$)	Contained in modes
$\mathbf{G}_Q(\mathbf{e}_x, \mathbf{e}_x, \mathbf{e}_x)$	B_{11}, B_{13}, B_{33}
$\mathbf{G}_Q(\mathbf{e}_y, \mathbf{e}_x, \mathbf{e}_x) = \mathbf{G}_Q(\mathbf{e}_x, \mathbf{e}_y, \mathbf{e}_x)$	$\tilde{B}_{11}, \tilde{B}_{13}, \tilde{B}_{33}, C_{12}$
$\mathbf{G}_Q(\mathbf{e}_z, \mathbf{e}_x, \mathbf{e}_x) = \mathbf{G}_Q(\mathbf{e}_x, \mathbf{e}_z, \mathbf{e}_x)$	$B_{01}, B_{03}, B_{23}, \tilde{C}_{22}$
$\mathbf{G}_Q(\mathbf{e}_y, \mathbf{e}_y, \mathbf{e}_x)$	$B_{11}, B_{13}, B_{33}, \tilde{C}_{12}$
$\mathbf{G}_Q(\mathbf{e}_z, \mathbf{e}_y, \mathbf{e}_x) = \mathbf{G}_Q(\mathbf{e}_y, \mathbf{e}_z, \mathbf{e}_x)$	$\tilde{B}_{23}, C_{22}, C_{02}$
$\mathbf{G}_Q(\mathbf{e}_z, \mathbf{e}_z, \mathbf{e}_x)$	$B_{11}, B_{13}, \tilde{C}_{12}$
$\mathbf{G}_Q(\mathbf{e}_x, \mathbf{e}_x, \mathbf{e}_y)$	$\tilde{B}_{11}, \tilde{B}_{13}, \tilde{B}_{33}, C_{12}$
$\mathbf{G}_Q(\mathbf{e}_y, \mathbf{e}_x, \mathbf{e}_y) = \mathbf{G}_Q(\mathbf{e}_x, \mathbf{e}_y, \mathbf{e}_y)$	$B_{11}, B_{13}, B_{33}, \tilde{C}_{12}$
$\mathbf{G}_Q(\mathbf{e}_z, \mathbf{e}_x, \mathbf{e}_y) = \mathbf{G}_Q(\mathbf{e}_x, \mathbf{e}_z, \mathbf{e}_y)$	$\tilde{B}_{23}, C_{22}, C_{02}$
$\mathbf{G}_Q(\mathbf{e}_y, \mathbf{e}_y, \mathbf{e}_y)$	$\tilde{B}_{11}, \tilde{B}_{13}, \tilde{B}_{33}$
$\mathbf{G}_Q(\mathbf{e}_z, \mathbf{e}_y, \mathbf{e}_y) = \mathbf{G}_Q(\mathbf{e}_y, \mathbf{e}_z, \mathbf{e}_y)$	$B_{01}, B_{03}, B_{23}, \tilde{C}_{22}$
$\mathbf{G}_Q(\mathbf{e}_z, \mathbf{e}_z, \mathbf{e}_y)$	$\tilde{B}_{11}, \tilde{B}_{13}, C_{12}$
$\mathbf{G}_Q(\mathbf{e}_x, \mathbf{e}_x, \mathbf{e}_z)$	$B_{01}, B_{03}, B_{23}, \tilde{C}_{22}$
$\mathbf{G}_Q(\mathbf{e}_y, \mathbf{e}_x, \mathbf{e}_z) = \mathbf{G}_Q(\mathbf{e}_x, \mathbf{e}_y, \mathbf{e}_z)$	\tilde{B}_{23}, C_{22}
$\mathbf{G}_Q(\mathbf{e}_z, \mathbf{e}_x, \mathbf{e}_z) = \mathbf{G}_Q(\mathbf{e}_x, \mathbf{e}_z, \mathbf{e}_z)$	$B_{11}, B_{13}, \tilde{C}_{12}$
$\mathbf{G}_Q(\mathbf{e}_y, \mathbf{e}_y, \mathbf{e}_z)$	$B_{01}, B_{03}, B_{23}, \tilde{C}_{22}$
$\mathbf{G}_Q(\mathbf{e}_z, \mathbf{e}_y, \mathbf{e}_z) = \mathbf{G}_Q(\mathbf{e}_y, \mathbf{e}_z, \mathbf{e}_z)$	$\tilde{B}_{11}, \tilde{B}_{13}, C_{12}$
$\mathbf{G}_Q(\mathbf{e}_z, \mathbf{e}_z, \mathbf{e}_z)$	B_{01}, B_{03}

Table 3 Correspondence between both rotlet dipoles and potential dipoles and different modes of squirring motion

Rotlet dipole ($\sim 1/r^3$)	Contained in modes	Source dipole ($\sim 1/r^3$)	Contained in modes
$\mathbf{R}_D(\mathbf{e}_x, \mathbf{e}_x)$	C_{02}, C_{22}	$\mathbf{P}_D(\mathbf{e}_x)$	B_{11}
$\mathbf{R}_D(\mathbf{e}_x, \mathbf{e}_y)$	B_{01}, \tilde{C}_{22}	$\mathbf{P}_D(\mathbf{e}_y)$	\tilde{B}_{11}
$\mathbf{R}_D(\mathbf{e}_x, \mathbf{e}_z)$	\tilde{B}_{11}, C_{12}	$\mathbf{P}_D(\mathbf{e}_z)$	B_{01}
$\mathbf{R}_D(\mathbf{e}_y, \mathbf{e}_x)$	B_{01}, \tilde{C}_{22}		
$\mathbf{R}_D(\mathbf{e}_y, \mathbf{e}_y)$	C_{02}, C_{22}		
$\mathbf{R}_D(\mathbf{e}_y, \mathbf{e}_z)$	B_{11}, \tilde{C}_{12}		
$\mathbf{R}_D(\mathbf{e}_z, \mathbf{e}_x)$	\tilde{B}_{11}, C_{12}		
$\mathbf{R}_D(\mathbf{e}_z, \mathbf{e}_y)$	B_{11}, \tilde{C}_{12}		
$\mathbf{R}_D(\mathbf{e}_z, \mathbf{e}_z)$	C_{02}		

include all possible configurations of the flow singularities (for different values of m in Eqs. (21)–(22)). From a physical point of view, the essential physics is therefore all contained in the case of the axisymmetric squirring motion, and the nonaxisymmetric flow fields are linear superpositions of flow singularities in different directions. For a given nonaxisymmetric squirring profile, the more general analysis in our paper provides a way to quantify, and understand, the general three-dimensional flow structure.

Finally, we note that in the axisymmetric case, Sect. 4.1, the translational and rotational velocities are always in the same direction, and hence an axisymmetric squirmer can only swim along a straight line (possibly in an unsteady fashion). This is generalized in the nonaxisymmetric case, where the motion of a steady squirmer is in general helical provided that $\mathbf{U} \cdot \boldsymbol{\Omega} \neq 0$. The special case

$$\mathbf{U} \cdot \boldsymbol{\Omega} = 0 \tag{72}$$

reduces the helical trajectory to a circle (a helix with zero pitch, Eq. (72)) while in the situation where

$$\mathbf{U} \times \boldsymbol{\Omega} = \mathbf{0}, \tag{73}$$

the trajectory is reduced to a straight line (a helix with zero radius, Eq. (73)). According to the swimming kinematics computed previously in Eqs. (60) and (61), and using Eqs. (58) and (59), we obtain that a squirmer performs a circular motion when

$$B_{11}C_{11} + \tilde{B}_{11}\tilde{C}_{11} + B_{01}C_{01} = 0, \quad (74)$$

while it follows a straight line when

$$\tilde{B}_{11}C_{01} - B_{01}\tilde{C}_{11} = B_{11}C_{01} - B_{01}C_{11} = B_{11}\tilde{C}_{11} - C_{11}\tilde{B}_{11} = 0. \quad (75)$$

4.4 Rate of work

In this section, the rate of work by the surface, \mathcal{P} , during a squirming motion is considered. In spherical coordinates, we write

$$\mathcal{P} = - \int_S \mathbf{n} \cdot \boldsymbol{\sigma} \cdot \mathbf{v} dS = - \int_0^{2\pi} \int_0^\pi (\sigma_{rr}v_r + \sigma_{r\theta}v_\theta + \sigma_{r\phi}v_\phi) \Big|_{r=a} a^2 \sin\theta d\theta d\phi. \quad (76)$$

The integrand can be evaluated with the Newtonian constitutive relation, $\boldsymbol{\sigma} = -p + \eta(\nabla\mathbf{v}^T + \nabla\mathbf{v})$, and the overall flow field of a swimming squirmer from Eqs. (62)–(64). After some lengthy manipulation, we find that, for purely tangential deformation, the rate of work for a general nonaxisymmetric squirming motion is given by the positive-definite formula

$$\begin{aligned} \mathcal{P} = & \frac{64\pi\eta}{3a^5} (B_{01}^2 + B_{11}^2 + \tilde{B}_{11}^2) + \sum_{n=2}^{\infty} \frac{4n(n+1)\pi\eta}{a^{2n+1}} \left(\frac{4}{n^2a^2} B_{0n}^2 + \frac{n+2}{2n+1} C_{0n}^2 \right) \\ & + \sum_{n=2}^{\infty} \sum_{m=1}^n \frac{2n(n+1)(n+m)!\pi\eta}{a^{2n+1}(n-m)!} \left[\frac{4}{n^2a} (B_{mn}^2 + \tilde{B}_{mn}^2) + \frac{n+2}{2n+1} (C_{mn}^2 + \tilde{C}_{mn}^2) \right]. \end{aligned} \quad (77)$$

Note that the identity

$$\int_{-1}^1 \left[(1-\mu^2)P_n^{m'}P_l^{m'} + m^2 \frac{P_n^m P_l^m}{1-\mu^2} \right] d\mu = \frac{2n(n+1)(n+m)!}{(2n+1)(n-m)!} \delta_{nl} \quad (78)$$

was derived and used in order to evaluate the necessary integrals in \mathcal{P} .

Using the result in Eq. (77), one can then compute the hydrodynamic efficiency of a swimming squirmer,

$$\mathcal{E} = \frac{6\pi\eta a \mathbf{U}^2}{\mathcal{P}}, \quad (79)$$

defined as the rate of work required to drag a spherical body at its swimming speed divided by the rate of work done by self-propulsion to produce the same swimming speed [63,64]. In the unsteady case, the efficiency is given by $6\pi\eta a \langle U \rangle^2 / \langle \mathcal{P} \rangle$, where $\langle \dots \rangle$ denotes time averaging. In Eq. (77) we see that all components contribute a positive rate of work. However, only the modes B_{01} , B_{11} , and \tilde{B}_{11} contribute to the propulsion of the squirmer (Eq. 60). In other words, the inclusion of any other squirming modes leads to less efficient swimming. The same holds in the axisymmetric case, where the expression for the rate of work reduces to

$$\mathcal{P} = \frac{64\pi\eta}{3a^5} B_{01}^2 + \sum_{n=2}^{\infty} \frac{4n(n+1)\pi\eta}{a^{2n+1}} \left(\frac{4}{n^2a^2} B_{0n}^2 + \frac{n+2}{2n+1} C_{0n}^2 \right), \quad (80)$$

a result that reduces to Blake's [41] in the case of purely tangential deformation, with the rescaling given by Eq. (25). Note that the results for the axisymmetric case here, Eq. (80), are more general because of the inclusion of the rate of work by the azimuthal but axisymmetric components C_{0n} that were not previously accounted for.

Interestingly, using the reciprocal theorem, Stone and Samuel [53] showed that the rate of work done by a general swimming organism is given by

$$\mathcal{P} = \eta \int_V \boldsymbol{\omega}^2 dV - 2\eta \int_S \mathbf{n} \cdot (\mathbf{v} \cdot \nabla \mathbf{v}) dS, \tag{81}$$

where $\boldsymbol{\omega}$ is the vorticity field in the fluid. Hence, for two swimmers propelling at the same speed, the one producing more vorticity dissipates more energy. It was therefore concluded that it is less efficient for an axisymmetric object to rotate as it swims compared with the corresponding nonrotating swimmer.

In the explicit expression of the rate of work in the axisymmetric case (Eq. 80), the modes causing rotation of the squirmer, C_{11} , \tilde{C}_{11} , and C_{01} , do not appear, which is not surprising given that these modes do not contribute to the flow field (see Eqs. (62)–(64) and Sect. 3.2 for explanations) due to zero apparent rotation from the perspective of the fluid. In other words, a squirmer that self-rotates by exploiting purely the C_{11} , \tilde{C}_{11} , or C_{01} mode induces no extra viscous dissipation. In this case, the swimmer rotates as it swims but it is as efficient as a nonrotating swimmer, simply because the rotational motion alone produces no net flow (or vorticity). In other words, no rotation is truly felt from the perspective of the fluid, even though from the perspective of the swimmer itself there is a nonzero rotation rate.

In general, however, a squirmer would have an azimuthal squirming profile containing not only the rotlet terms but also other modes C_{mn} ($n \geq 2$), which would dissipate more energy, making the swimmer less efficient according to Eq. (80). The body rotation is apparent from the perspective of the fluid only when the azimuthal squirming profile contains modes C_{mn} ($n \geq 2$) other than the rotlet terms, hence the conclusion by Stone and Samuel [53].

4.5 Squirming with arbitrary surface velocities

In previous sections, the surface velocities were expressed in the form of the boundary values of Lamb’s general solution, Eqs. (58) and (59), and the flow structure under such a decomposition was discussed. In general however, the surface velocities could be more naturally described using other surface decompositions. Here, we detail how to relate surface velocities expressed in arbitrary forms to the decomposition employed in Lamb’s general solution.

For illustration, we decompose the arbitrary surface velocities in natural Fourier modes along the azimuthal direction ϕ as

$$\mathbf{u}(a, \theta, \phi) = \sum_{m=0}^{\infty} \left[E_m(\theta) \cos m\phi + \tilde{E}_m(\theta) \sin m\phi \right] \mathbf{e}_\theta + \sum_{m=0}^{\infty} \left[F_m(\theta) \cos m\phi + \tilde{F}_m(\theta) \sin m\phi \right] \mathbf{e}_\phi, \tag{82}$$

where $E_m(\theta)$, $\tilde{E}_m(\theta)$, $F_m(\theta)$, $\tilde{F}_m(\theta)$ are arbitrary functions in the polar direction projected from the boundary actuation under this decomposition. The goal here is therefore to derive the set of coefficients, A_{mn} , \tilde{A}_{mn} , B_{mn} , \tilde{B}_{mn} , C_{mn} , \tilde{C}_{mn} , in Lamb’s general solution, Eqs. (58) and (59), given the surface velocities expressed in Eq. (82).

The attempt to directly project Eq. (82) onto Eqs. (58) and (59) to calculate the coefficients is nontrivial because a mix of basis functions is used in Eq. (58) and (59), and there is no obvious way of doing orthogonal projections to calculate the coefficients (unless $m = 0$ for the axisymmetric case). We instead follow a systematic scheme due to Brenner [56], facilitating the projections of boundary conditions when using Lamb’s general solution. While the radial velocity on the sphere is still matched, in place of matching the polar and azimuthal velocity components on the sphere, the quantities $r(\nabla \cdot \mathbf{u}|_{r=a})$ and $r\mathbf{e}_r \cdot (\nabla \times \mathbf{u}|_{r=a})$ are matched [56,57,65], leading to

$$\mathbf{e}_r \cdot \mathbf{u}|_{r=a} = \sum_{n=1}^{\infty} \left[\frac{(n+1)ap_{-(n+1)}|_{r=a}}{2\eta(2n-1)} - \frac{n+1}{a} \Phi_{-(n+1)}|_{r=a} \right], \tag{83}$$

$$-r\nabla \cdot (\mathbf{u}|_{r=a}) = \sum_{n=1}^{\infty} \left[-\frac{n(n+1)a}{2\eta(2n-1)} p_{-(n+1)}|_{r=a} + \frac{(n+1)(n+2)}{a} \Phi_{-(n+1)}|_{r=a} \right], \tag{84}$$

$$r\mathbf{e}_r \cdot (\nabla \times \mathbf{u}|_{r=a}) = \sum_{n=1}^{\infty} n(n+1)\chi_{-(n+1)}|_{r=a}, \tag{85}$$

in terms of Lamb's general solution.

In the case of the purely tangential deformation, the first matching condition, Eq. (83), is simply the conditions for no radial deformation, Eq. (19), relating B_{mn} and \tilde{B}_{mn} to A_{mn} and \tilde{A}_{mn} . We are therefore left only with Eqs. (84) and (85) to determine the remaining coefficients. Expressed in spherical coordinates, Eqs. (84) and (85) are written as

$$-2 u_r|_{r=a} - \frac{1}{\sin \theta} \left[\frac{\partial}{\partial \theta} (u_\theta \sin \theta) + \frac{\partial u_\phi}{\partial \phi} \right]_{r=a} = \sum_{n=1}^{\infty} \sum_{m=0}^n \frac{2(n+1)}{a^{n+2}} P_n^m \left(B_{mn} \cos m\phi + \tilde{B}_{mn} \sin m\phi \right), \quad (86)$$

$$\frac{1}{\sin \theta} \left[\frac{\partial}{\partial \theta} (u_\phi \sin \theta) - \frac{\partial u_\theta}{\partial \phi} \right]_{r=a} = \sum_{n=1}^{\infty} \sum_{m=0}^n \frac{n(n+1)}{a^{n+1}} P_n^m \left(C_{mn} \cos m\phi + \tilde{C}_{mn} \sin m\phi \right). \quad (87)$$

The benefits of Brenner's matching conditions are now clear because the coefficients on the right-hand side of Eqs. (86) and (87) can be readily determined by the orthogonality of the associated Legendre polynomials. Substituting the prescribed boundary conditions, Eq. (82), into the preceding matching conditions yields the two equations

$$\begin{aligned} & \frac{1}{\sin \theta} \frac{\partial}{\partial \theta} (E_0 \sin \theta) - \sum_{m=1}^{\infty} \left\{ \left[\frac{1}{\sin \theta} \frac{\partial}{\partial \theta} (E_m \sin \theta) + m \frac{\tilde{F}_m}{\sin \theta} \right] \cos m\phi + \left[\frac{1}{\sin \theta} \frac{\partial}{\partial \theta} (\tilde{E}_m \sin \theta) + m \frac{F_m}{\sin \theta} \right] \sin m\phi \right\} \\ & = \sum_{n=1}^{\infty} \frac{2(n+1)}{a^{n+2}} P_n B_{0n} + \sum_{n=1}^{\infty} \sum_{m=n}^{\infty} \frac{2(n+1)}{a^{n+2}} P_n^m \left(B_{mn} \cos m\phi + \tilde{B}_{mn} \sin m\phi \right), \end{aligned} \quad (88)$$

$$\begin{aligned} & \frac{1}{\sin \theta} \frac{\partial}{\partial \theta} (F_0 \sin \theta) + \sum_{n=1}^{\infty} \frac{1}{\sin \theta} \left\{ \left[\frac{\partial}{\partial \theta} (F_m \sin \theta) - m \tilde{E}_m \right] \cos m\phi + \left[\frac{\partial}{\partial \theta} (\tilde{F}_m \sin \theta) + m E_m \right] \sin m\phi \right\} \\ & = \sum_{n=1}^{\infty} \frac{n(n+1)}{a^{n+1}} P_n C_{0n} + \sum_{m=1}^{\infty} \sum_{n=m}^{\infty} \frac{n(n+1)}{a^{n+1}} P_n^m \left(C_{mn} \cos m\phi + \tilde{C}_{mn} \sin m\phi \right). \end{aligned} \quad (89)$$

Finally, by the orthogonality of the associated Legendre polynomials we obtain the remaining explicit expressions for the Lamb coefficients as

$$B_{mn} = \frac{a^{n+2}}{4} \frac{(2n+1)(n-m)!}{(n+1)(n+m)!} \int_{-1}^1 \left[\frac{\partial}{\partial \mu} (E_m \sin \theta) - \frac{m \tilde{F}_m}{\sin \theta} \right] P_n^m d\mu, \quad (90)$$

$$\tilde{B}_{mn} = \frac{a^{n+2}}{4} \frac{(2n+1)(n-m)!}{(n+1)(n+m)!} \int_{-1}^1 \left[\frac{\partial}{\partial \mu} (\tilde{E}_m \sin \theta) + \frac{m F_m}{\sin \theta} \right] P_n^m d\mu, \quad (91)$$

$$C_{mn} = \frac{a^{n+1}}{2n} \frac{(2n+1)(n-m)!}{(n+1)(n+m)!} \int_{-1}^1 \left[-\frac{\partial}{\partial \mu} (F_m \sin \theta) - \frac{m \tilde{E}_m}{\sin \theta} \right] P_n^m d\mu, \quad (92)$$

$$\tilde{C}_{mn} = \frac{a^{n+1}}{2n} \frac{(2n+1)(n-m)!}{(n+1)(n+m)!} \int_{-1}^1 \left[-\frac{\partial}{\partial \mu} (\tilde{F}_m \sin \theta) + \frac{m E_m}{\sin \theta} \right] P_n^m d\mu, \quad (93)$$

for $0 \leq m \leq \infty$ and $m \leq n \neq 0$. Note that the coefficients A_{mn} and \tilde{A}_{mn} are given by the purely tangential deformation conditions, Eq. (19). A more general analysis, including radial deformation at the squirmer surface, is presented in Appendix D.

5 Discussion

In this paper, we have investigated the squirring motion of a sphere using Lamb's general solution. With this alternative formulation, our results first completed the classical analysis of axisymmetric squirring motion by

including the azimuthal velocity fields not taken into account in previous studies (Sect. 3). We then extended the analysis to the general nonaxisymmetric case in order to study the motion of a squirmer performing arbitrary three-dimensional translation and rotation (Sect. 4). Analytical formulae for both the swimming kinematics and the complete flow field were derived (Sect. 4.1). In the axisymmetric case, the motion of a squirmer is restricted to a straight line, and removing the axisymmetry frees the squirmer to move with helical trajectories in general, with circular and straight paths as special limits.

As summarized in Sect. 4.2, the swimming kinematics of arbitrary squirming profiles can be obtained using a reciprocal theorem approach. However, that approach does not allow us to gain information on the flow induced by the squirmer, which is important for the computation of the swimmer hydrodynamic efficiency and for problems such as the transport and uptake of nutrients of microorganisms. In our paper, we obtained the flow field around the squirmer analytically using Lamb’s general solution, and we interpreted the flow structure in terms of fundamental singularities in Stokes flows (Sect. 4.3). We also remarked on the power dissipation and efficiency of a generalized squirmer (Sect. 4.4) and detailed the general procedure of relating surface velocities of arbitrary forms to the form used in Lamb’s general solution (Sect. 4.5).

The traditional, axisymmetric squirmer model has been widely adopted to describe pushers and pullers by changing the sign of the stresslet component relative to the source dipole (B_{02}/B_{01}), thereby making it possible to address many problems in biological physics (as detailed in the introduction). With the axisymmetric azimuthal modes identified in this work, the squirmer model may, for instance, be modified to incorporate a rotlet dipole to represent the effect of the rotating cell body and the counterrotating flagellum of *Escherichia coli*. The freedom to choose the sign of the rotlet dipole relative to the source dipole (C_{02}/B_{01}) may also be useful in the study of the switching of rotation direction in bacterial flagella during tumbling processes [66]. Higher-order, nonaxisymmetric modes may now also be included to model more complex hydrodynamic effects. This generalized squirmer model may then be useful for investigating three-dimensional swimmer–swimmer or swimmer–boundary interactions.

Acknowledgments Funding from the US National Science Foundation (Grant CBET-0746285 to E.L.) and the Croucher Foundation (through a fellowship to O.S.P.) is gratefully acknowledged. The authors also wish to thank the Department of Mechanical and Aerospace Engineering at the University of California, San Diego where this work was initiated.

Appendix A: Fundamental flow singularities in spherical coordinates

A.1 Stokeslets

The solution to Stokes equations due to a point force $f\boldsymbol{\alpha}\delta(\mathbf{r})$ of magnitude f , and the direction $\boldsymbol{\alpha}$ at the origin is given by $\mathbf{u} = f\mathbf{G}(\boldsymbol{\alpha})/(8\pi\eta)$, where the vectorial representation of a Stokeslet is given by Eq. (36) in the main text.

Note that $\boldsymbol{\alpha}$ denotes the direction of the Stokeslet. Stokeslets in different Cartesian directions are expressed in spherical coordinates as

$$\mathbf{G}(\mathbf{e}_x) = \frac{1}{r} [2 \sin \theta \cos \phi \mathbf{e}_r + \cos \theta \cos \phi \mathbf{e}_\theta - \sin \phi \mathbf{e}_\phi], \tag{94}$$

$$\mathbf{G}(\mathbf{e}_y) = \frac{1}{r} [2 \sin \theta \sin \phi \mathbf{e}_r + \cos \theta \sin \phi \mathbf{e}_\theta + \cos \phi \mathbf{e}_\phi], \tag{95}$$

$$\mathbf{G}(\mathbf{e}_z) = \frac{1}{r} [2 \cos \theta \mathbf{e}_r - \sin \theta \mathbf{e}_\theta]. \tag{96}$$

A.2 A general Stokes dipole

A general force dipole is obtained by taking the derivative of a Stokeslet along the direction of interest. The vectorial representation of a force dipole is given by Eq. (44) in the main text, where $\boldsymbol{\alpha}$ and $\boldsymbol{\beta}$ denote respectively the direction

of the Stokeslet and the direction along which the derivative is taken. The expressions of Stokes dipoles of different configurations in spherical coordinates are given by

$$\mathbf{G}_D(\mathbf{e}_x, \mathbf{e}_x) = \frac{1}{r^2} \left[-\frac{1}{4}(1 + 3 \cos 2\theta) + \frac{3}{4}(1 - \cos 2\theta) \cos 2\phi \right] \mathbf{e}_r, \quad (97)$$

$$\mathbf{G}_D(\mathbf{e}_y, \mathbf{e}_y) = \frac{1}{r^2} \left[-\frac{1}{4}(1 + 3 \cos 2\theta) - \frac{3}{4}(1 - \cos 2\theta) \cos 2\phi \right] \mathbf{e}_r, \quad (98)$$

$$\mathbf{G}_D(\mathbf{e}_z, \mathbf{e}_z) = \frac{1}{2r^2}(1 + 3 \cos 2\theta) \mathbf{e}_r, \quad (99)$$

$$\mathbf{G}_D(\mathbf{e}_y, \mathbf{e}_x) = \frac{1}{r^2} \left[\frac{3}{4}(1 - \cos 2\theta) \sin 2\phi \mathbf{e}_r - \sin \theta \mathbf{e}_\phi \right], \quad (100)$$

$$\mathbf{G}_D(\mathbf{e}_z, \mathbf{e}_x) = \frac{1}{r^2} \left(\frac{3}{2} \sin 2\theta \cos \phi \mathbf{e}_r + \cos \phi \mathbf{e}_\theta - \cos \theta \sin \phi \mathbf{e}_\phi \right), \quad (101)$$

$$\mathbf{G}_D(\mathbf{e}_x, \mathbf{e}_y) = \frac{1}{r^2} \left[\frac{3}{4}(1 - \cos 2\theta) \sin 2\phi \mathbf{e}_r + \sin \theta \mathbf{e}_\phi \right], \quad (102)$$

$$\mathbf{G}_D(\mathbf{e}_z, \mathbf{e}_y) = \frac{1}{r^2} \left(\frac{3}{2} \sin 2\theta \sin \phi \mathbf{e}_r + \sin \phi \mathbf{e}_\theta + \cos \theta \cos \phi \mathbf{e}_\phi \right), \quad (103)$$

$$\mathbf{G}_D(\mathbf{e}_x, \mathbf{e}_z) = \frac{1}{r^2} \left(\frac{3}{2} \sin 2\theta \cos \phi \mathbf{e}_r - \cos \phi \mathbf{e}_\theta + \cos \theta \sin \phi \mathbf{e}_\phi \right), \quad (104)$$

$$\mathbf{G}_D(\mathbf{e}_y, \mathbf{e}_z) = \frac{1}{r^2} \left(\frac{3}{2} \sin 2\theta \sin \phi \mathbf{e}_r - \sin \phi \mathbf{e}_\theta - \cos \theta \cos \phi \mathbf{e}_\phi \right). \quad (105)$$

A.3 Stresslets

The vectorial representation of a stresslet is given by Eq. (45) in the main text, where $\boldsymbol{\alpha}$ and $\boldsymbol{\beta}$ denote respectively the direction of the Stokeslet and the direction along which the derivative is taken. The expressions of stresslets of different configurations in spherical coordinates are given by

$$\mathbf{S}(\mathbf{e}_x, \mathbf{e}_x) = \mathbf{G}_D(\mathbf{e}_x, \mathbf{e}_x) = \frac{1}{r^2} \left[-\frac{1}{4}(1 + 3 \cos 2\theta) + \frac{3}{4}(1 - \cos 2\theta) \cos 2\phi \right] \mathbf{e}_r, \quad (106)$$

$$\mathbf{S}(\mathbf{e}_y, \mathbf{e}_y) = \mathbf{G}_D(\mathbf{e}_y, \mathbf{e}_y) = \frac{1}{r^2} \left[-\frac{1}{4}(1 + 3 \cos 2\theta) - \frac{3}{4}(1 - \cos 2\theta) \cos 2\phi \right] \mathbf{e}_r, \quad (107)$$

$$\mathbf{S}(\mathbf{e}_z, \mathbf{e}_z) = \mathbf{G}_D(\mathbf{e}_z, \mathbf{e}_z) = \frac{1}{2r^2}(1 + 3 \cos 2\theta) \mathbf{e}_r, \quad (108)$$

$$\mathbf{S}(\mathbf{e}_y, \mathbf{e}_x) = \mathbf{S}(\mathbf{e}_x, \mathbf{e}_y) = \frac{3}{4r^2}(1 - \cos 2\theta) \sin 2\phi \mathbf{e}_r, \quad (109)$$

$$\mathbf{S}(\mathbf{e}_z, \mathbf{e}_x) = \mathbf{S}(\mathbf{e}_x, \mathbf{e}_z) = \frac{3}{2r^2} \sin 2\theta \cos \phi \mathbf{e}_r, \quad (110)$$

$$\mathbf{S}(\mathbf{e}_z, \mathbf{e}_y) = \mathbf{S}(\mathbf{e}_y, \mathbf{e}_z) = \frac{3}{2r^2} \sin 2\theta \sin \phi \mathbf{e}_r. \quad (111)$$

A.4 Rotlets

The vectorial representation of a rotlet is given by Eq. (46) in the main text, where $\boldsymbol{\zeta} = \boldsymbol{\beta} \times \boldsymbol{\alpha}$ denotes the direction of the rotlet. The expressions of rotlets in different directions in spherical coordinates are given by

$$\mathbf{R}(\mathbf{e}_x) = \frac{1}{r^2} (-\sin \phi \mathbf{e}_\theta - \cos \theta \cos \phi \mathbf{e}_\phi), \tag{112}$$

$$\mathbf{R}(\mathbf{e}_y) = \frac{1}{r^2} (\cos \phi \mathbf{e}_\theta - \cos \theta \sin \phi \mathbf{e}_\phi), \tag{113}$$

$$\mathbf{R}(\mathbf{e}_z) = \frac{1}{r^2} (\sin \theta \mathbf{e}_\phi). \tag{114}$$

A.5 A general Stokes quadrupole

A higher-order singularity, the force quadrupole, is obtained by taking the derivative of a force dipole along different directions and is given by Eq. (50) in the main text, where $\boldsymbol{\beta}, \boldsymbol{\gamma}$ are the directions along which each derivative is taken. The expressions of Stokes quadrupoles of different configurations in spherical coordinates are given by

$$\begin{aligned} \mathbf{G}(\mathbf{e}_x, \mathbf{e}_x, \mathbf{e}_x) &= \frac{1}{4r^3} [-5 \sin \theta + 9 \sin 3\theta] \cos \phi + 3(3 \sin \theta - \sin 3\theta) \cos 3\phi \mathbf{e}_r \\ &\quad + \frac{1}{16r^3} [(7 \cos \theta + 9 \cos 3\theta) \cos \phi - 3(\cos \theta - \cos 3\theta) \cos 3\phi] \mathbf{e}_\theta \\ &\quad + \frac{1}{8r^3} [-5 + 3 \cos 2\theta] \sin \phi + 3(1 - \cos 2\theta) \sin 3\phi \mathbf{e}_\phi, \end{aligned} \tag{115}$$

$$\begin{aligned} \mathbf{G}(\mathbf{e}_y, \mathbf{e}_x, \mathbf{e}_x) &= \mathbf{G}(\mathbf{e}_x, \mathbf{e}_y, \mathbf{e}_x) \\ &= \frac{1}{4r^3} [(\sin \theta - 3 \sin 3\theta) \sin \phi + 3(3 \sin \theta - \sin 3\theta) \sin 3\phi] \mathbf{e}_r \\ &\quad + \frac{1}{16r^3} [(13 \cos \theta + 3 \cos 3\theta) \sin \phi + 3(\cos 3\theta - \cos \theta) \sin 3\phi] \mathbf{e}_\theta \\ &\quad + \frac{1}{8r^3} [(9 \cos 2\theta - 1) \cos \phi - 3(1 - \cos 2\theta) \cos 3\phi] \mathbf{e}_\phi, \end{aligned} \tag{116}$$

$$\begin{aligned} \mathbf{G}(\mathbf{e}_z, \mathbf{e}_x, \mathbf{e}_x) &= \mathbf{G}(\mathbf{e}_x, \mathbf{e}_z, \mathbf{e}_x) \\ &= \frac{1}{2r^3} [-(\cos \theta + 3 \cos 3\theta) + 3(\cos \theta - \cos 3\theta) \cos 2\phi] \mathbf{e}_r \\ &\quad + \frac{1}{8r^3} [(\sin \theta - 3 \sin 3\theta) + 3(3 \sin \theta - \sin 3\theta) \cos 2\phi] \mathbf{e}_\theta, \end{aligned} \tag{117}$$

$$\begin{aligned} \mathbf{G}(\mathbf{e}_y, \mathbf{e}_y, \mathbf{e}_x) &= \frac{1}{4r^3} [-(7 \sin \theta + 3 \sin 3\theta) \cos \phi - 3(3 \sin \theta - \sin 3\theta) \cos 3\phi] \mathbf{e}_r \\ &\quad + \frac{1}{16r^3} [(3 \cos 3\theta - 19 \cos \theta) \cos \phi + 3(\cos \theta - \cos 3\theta) \cos 3\phi] \mathbf{e}_\theta \\ &\quad + \frac{1}{8r^3} [(15 \cos 2\theta - 7) \sin \phi - 3(1 - \cos 2\theta) \sin 3\phi] \mathbf{e}_\phi, \end{aligned} \tag{118}$$

$$\begin{aligned} \mathbf{G}(\mathbf{e}_z, \mathbf{e}_y, \mathbf{e}_x) &= \mathbf{G}(\mathbf{e}_y, \mathbf{e}_z, \mathbf{e}_x) \\ &= \frac{1}{r^3} \left[\frac{3}{2} (\cos \theta - \cos 3\theta) \sin 2\phi \mathbf{e}_r + \frac{3}{8} (3 \sin \theta - \sin 3\theta) \sin 2\phi \mathbf{e}_\theta - \frac{3}{2} \sin 2\theta \mathbf{e}_\phi \right], \end{aligned} \tag{119}$$

$$\begin{aligned} \mathbf{G}(\mathbf{e}_z, \mathbf{e}_z, \mathbf{e}_x) &= \frac{1}{r^3} \left[(3 \sin 3\theta - \sin \theta) \cos \phi \mathbf{e}_r + \frac{1}{4} (11 \cos \theta - 3 \cos 3\theta) \cos \phi \mathbf{e}_\theta \right. \\ &\quad \left. - \frac{1}{2} (1 + 3 \cos 2\theta) \sin \phi \mathbf{e}_\phi \right], \end{aligned} \tag{120}$$

$$\begin{aligned} \mathbf{G}(\mathbf{e}_x, \mathbf{e}_x, \mathbf{e}_y) &= \frac{1}{4r^3} [-(7 \sin \theta + 3 \sin 3\theta) \sin \phi + 3(3 \sin \theta - \sin 3\theta) \sin 3\phi] \mathbf{e}_r \\ &\quad + \frac{1}{16r^3} [\cos \theta (-19 + 3 \cos 2\theta) \sin \phi - 3(\cos \theta - \cos 3\theta) \sin 3\phi] \mathbf{e}_\theta \\ &\quad + \frac{1}{8r^3} [(7 - 15 \cos 2\theta) \cos \phi - 3(1 - \cos 2\theta) \cos 3\phi] \mathbf{e}_\phi, \end{aligned} \tag{121}$$

$$\begin{aligned}
\mathbf{G}(\mathbf{e}_y, \mathbf{e}_x, \mathbf{e}_y) &= \mathbf{G}(\mathbf{e}_x, \mathbf{e}_y, \mathbf{e}_y) \\
&= \frac{1}{4r^3} [(\sin \theta - 3 \sin 3\theta) \cos \phi - 3(3 \sin \theta - \sin 3\theta) \cos 3\phi] \mathbf{e}_r \\
&\quad + \frac{1}{16r^3} [(13 \cos \theta + 3 \cos 3\theta) \cos \phi + 3(\cos \theta - \cos 3\theta) \cos 3\phi] \mathbf{e}_\theta \\
&\quad + \frac{1}{8r^3} [(1 - 9 \cos 2\theta) \sin \phi - 3(1 - \cos 2\theta) \sin 3\phi] \mathbf{e}_\phi, \tag{122}
\end{aligned}$$

$$\begin{aligned}
\mathbf{G}(\mathbf{e}_z, \mathbf{e}_x, \mathbf{e}_y) &= \mathbf{G}(\mathbf{e}_x, \mathbf{e}_z, \mathbf{e}_y) \\
&= \frac{1}{r^3} \left[\frac{3}{2} (\cos \theta - \cos 3\theta) \sin 2\phi \mathbf{e}_r + \frac{3}{8} (3 \sin \theta - \sin 3\theta) \sin 2\phi \mathbf{e}_\theta + \frac{3}{2} \sin 2\theta \mathbf{e}_\phi \right], \tag{123}
\end{aligned}$$

$$\begin{aligned}
\mathbf{G}(\mathbf{e}_y, \mathbf{e}_y, \mathbf{e}_y) &= \frac{1}{4r^3} [-(5 \sin \theta + 9 \sin 3\theta) \sin \phi - 3(3 \sin \theta - \sin 3\theta) \sin 3\phi] \mathbf{e}_r \\
&\quad + \frac{1}{16r^3} [(7 \cos \theta + 9 \cos 3\theta) \sin \phi + 3(\cos \theta - \cos 3\theta) \sin 3\phi] \mathbf{e}_\theta \\
&\quad + \frac{1}{8r^3} [(5 + 3 \cos 2\theta) \cos \phi + 3(1 - \cos 2\theta) \cos 3\phi] \mathbf{e}_\phi, \tag{124}
\end{aligned}$$

$$\begin{aligned}
\mathbf{G}(\mathbf{e}_z, \mathbf{e}_y, \mathbf{e}_y) &= \mathbf{G}(\mathbf{e}_y, \mathbf{e}_z, \mathbf{e}_y) \\
&= \frac{1}{2r^3} [-(\cos \theta + 3 \cos 3\theta) - 3(\cos \theta - \cos 3\theta) \cos 2\phi] \mathbf{e}_r \\
&\quad + \frac{1}{8r^3} [(\sin \theta - 3 \sin 3\theta) - 3(3 \sin \theta - \sin 3\theta) \cos 2\phi] \mathbf{e}_\theta, \tag{125}
\end{aligned}$$

$$\begin{aligned}
\mathbf{G}(\mathbf{e}_z, \mathbf{e}_z, \mathbf{e}_y) &= \frac{1}{r^3} \left[(3 \sin \theta - \sin \theta) \sin \phi \mathbf{e}_r + \frac{1}{4} (11 \cos \theta - 3 \cos 3\theta) \sin \phi \mathbf{e}_\theta \right. \\
&\quad \left. + \frac{1}{2} (1 + 3 \cos 2\theta) \cos \phi \mathbf{e}_\phi \right], \tag{126}
\end{aligned}$$

$$\begin{aligned}
\mathbf{G}(\mathbf{e}_x, \mathbf{e}_x, \mathbf{e}_z) &= \frac{1}{2r^3} [-(5 \cos \theta + 3 \cos 3\theta) + 3(\cos \theta - \cos 3\theta) \cos 2\phi] \mathbf{e}_r \\
&\quad - \frac{1}{8r^3} [(7 \sin \theta + 3 \sin 3\theta) + 3(5 \sin \theta + \sin 3\theta) \cos 2\phi] \mathbf{e}_\theta + \frac{3}{2r^3} \sin 2\theta \sin 2\phi \mathbf{e}_\phi, \tag{127}
\end{aligned}$$

$$\begin{aligned}
\mathbf{G}(\mathbf{e}_y, \mathbf{e}_x, \mathbf{e}_z) &= \mathbf{G}(\mathbf{e}_x, \mathbf{e}_y, \mathbf{e}_z) \\
&= \frac{1}{r^3} \left[\frac{3}{2} (\cos \theta - \cos 3\theta) \sin 2\phi \mathbf{e}_r - \frac{3}{8} (5 \sin \theta + \sin 3\theta) \sin 2\phi \mathbf{e}_\theta - \frac{3}{2} \sin 2\theta \cos 2\phi \mathbf{e}_\phi \right], \tag{128}
\end{aligned}$$

$$\begin{aligned}
\mathbf{G}(\mathbf{e}_z, \mathbf{e}_x, \mathbf{e}_z) &= \mathbf{G}(\mathbf{e}_x, \mathbf{e}_z, \mathbf{e}_z) \\
&= \frac{1}{r^3} \left[(\sin \theta + 3 \sin 3\theta) \cos \phi \mathbf{e}_r - \frac{1}{4} (5 \cos \theta + 3 \cos 3\theta) \cos \phi \mathbf{e}_\theta + \frac{1}{2} (1 + 3 \cos 2\theta) \mathbf{e}_\phi \right], \tag{129}
\end{aligned}$$

$$\begin{aligned}
\mathbf{G}(\mathbf{e}_y, \mathbf{e}_y, \mathbf{e}_z) &= \frac{1}{2r^3} [-(5 \cos \theta + 3 \cos 3\theta) - 3(\cos \theta - \cos 3\theta) \cos 2\phi] \mathbf{e}_r \\
&\quad + \frac{1}{8r^3} [-(7 \sin \theta + 3 \sin 3\theta) + 3(5 \sin \theta + \sin 3\theta) \cos 2\phi] \mathbf{e}_\theta - \frac{3}{2r^3} \sin 2\theta \sin 2\phi \mathbf{e}_\phi, \tag{130}
\end{aligned}$$

$$\begin{aligned}
\mathbf{G}(\mathbf{e}_z, \mathbf{e}_y, \mathbf{e}_z) &= \mathbf{G}(\mathbf{e}_y, \mathbf{e}_z, \mathbf{e}_z) \\
&= \frac{1}{r^3} \left[(\sin \theta + 3 \sin 3\theta) \sin \phi \mathbf{e}_r - \frac{1}{4} (5 \cos \theta + 3 \cos 3\theta) \sin \phi \mathbf{e}_\theta - \frac{1}{2} (1 + 3 \cos 2\theta) \cos \phi \mathbf{e}_\phi \right], \tag{131}
\end{aligned}$$

$$\begin{aligned}
\mathbf{G}(\mathbf{e}_z, \mathbf{e}_z, \mathbf{e}_z) &= \frac{1}{r^3} \left[(\cos \theta + 3 \cos 3\theta) \mathbf{e}_r + \frac{1}{4} (3 \sin 3\theta - \sin \theta) \mathbf{e}_\theta \right]. \tag{132}
\end{aligned}$$

A.6 Potential dipoles

The vectorial representation of a potential (source) dipole is given by Eq. (52) in the main text, where α denotes the direction of the dipole. The expressions of potential dipoles in different directions in spherical coordinates are given by

$$\mathbf{P}_D(\mathbf{e}_x) = \frac{1}{r^3} [2 \sin \theta \cos \phi \mathbf{e}_r - \cos \theta \cos \phi \mathbf{e}_\theta + \sin \phi \mathbf{e}_\phi], \tag{133}$$

$$\mathbf{P}_D(\mathbf{e}_y) = \frac{1}{r^3} [2 \sin \theta \sin \phi \mathbf{e}_r - \cos \theta \sin \phi \mathbf{e}_\theta - \cos \phi \mathbf{e}_\phi], \tag{134}$$

$$\mathbf{P}_D(\mathbf{e}_z) = \frac{1}{r^3} [2 \cos \theta \mathbf{e}_r + \sin \theta \mathbf{e}_\theta]. \tag{135}$$

A.7 Rotlet dipoles

One can take a derivative of a rotlet to obtain a rotlet dipole, which is given by Eq. (56) in the main text, where ζ and γ denote respectively the direction of the rotlet and the direction along which the derivative is taken. The expressions of rotlet dipoles of different configurations in spherical coordinates are given by

$$\mathbf{R}_D(\mathbf{e}_x, \mathbf{e}_x) = \frac{1}{r^3} \left[-\frac{3}{2} \sin \theta \sin 2\phi \mathbf{e}_\theta - \frac{3}{4} \sin 2\theta (1 + \cos 2\phi) \mathbf{e}_\phi \right], \tag{136}$$

$$\mathbf{R}_D(\mathbf{e}_y, \mathbf{e}_y) = \frac{1}{r^3} \left[\frac{3}{2} \sin \theta \sin 2\phi \mathbf{e}_\theta - \frac{3}{4} \sin 2\theta (1 - \cos 2\phi) \mathbf{e}_\phi \right], \tag{137}$$

$$\mathbf{R}_D(\mathbf{e}_z, \mathbf{e}_z) = \frac{3 \sin 2\theta}{2r^3} \mathbf{e}_\phi, \tag{138}$$

$$\mathbf{R}_D(\mathbf{e}_y, \mathbf{e}_x) = \frac{1}{r^3} \left[-\cos \theta \mathbf{e}_r - \frac{1}{2} \sin \theta (1 - 3 \cos 2\phi) \mathbf{e}_\theta - \frac{3}{4} \sin 2\theta \sin 2\phi \mathbf{e}_\phi \right], \tag{139}$$

$$\mathbf{R}_D(\mathbf{e}_z, \mathbf{e}_x) = \frac{1}{r^3} \left[\sin \theta \sin \phi \mathbf{e}_r - 2 \cos \theta \sin \phi \mathbf{e}_\theta - \frac{1}{2} (1 + 3 \cos 2\theta) \cos \phi \mathbf{e}_\phi \right], \tag{140}$$

$$\mathbf{R}_D(\mathbf{e}_x, \mathbf{e}_y) = \frac{1}{r^3} \left[\cos \theta \mathbf{e}_r + \frac{1}{2} \sin \theta (1 + 3 \cos 2\phi) \mathbf{e}_\theta - \frac{3}{4} \sin 2\theta \sin 2\phi \mathbf{e}_\phi \right], \tag{141}$$

$$\mathbf{R}_D(\mathbf{e}_z, \mathbf{e}_y) = \frac{1}{r^3} \left[-\sin \theta \cos \phi \mathbf{e}_r + 2 \cos \theta \cos \phi \mathbf{e}_\theta - \frac{1}{2} (1 + 3 \cos 2\theta) \sin \phi \mathbf{e}_\phi \right], \tag{142}$$

$$\mathbf{R}_D(\mathbf{e}_x, \mathbf{e}_z) = \frac{1}{r^3} \left[-\sin \theta \sin \phi \mathbf{e}_r - \cos \theta \sin \phi \mathbf{e}_\theta + \frac{1}{2} (1 - 3 \cos 2\theta) \cos \phi \mathbf{e}_\phi \right], \tag{143}$$

$$\mathbf{R}_D(\mathbf{e}_y, \mathbf{e}_z) = \frac{1}{r^3} \left[\sin \theta \cos \phi \mathbf{e}_r + \cos \theta \cos \phi \mathbf{e}_\theta + \frac{1}{2} (1 - 3 \cos 2\theta) \sin \phi \mathbf{e}_\phi \right]. \tag{144}$$

Appendix B: Swimming of a squirmer with radial deformation

In the main text, we considered squirmers with a purely tangential deformation. In this appendix, we complement these results by addressing the case of squirmers also undergoing radial deformation. The results here might also be useful for modeling jet-driven microscopic swimmers, for instance, the locomotion of bacteria expelling slime.

For the axisymmetric case without the restriction to purely tangential deformations, Eq. (19), the solution to the pumping problem reads

$$u_r = \sum_{n=1}^{\infty} \frac{(n+1)P_n}{2(2n-1)\eta r^{n+2}} [A_{0n}r^2 - 2B_{0n}(2n-1)\eta], \tag{145}$$

$$u_\theta = \sum_{n=1}^{\infty} \frac{\sin \theta P'_n}{2r^n} \left[\frac{n-2}{n(2n-1)\eta} A_{0n} - \frac{2}{r^2} B_{0n} \right], \tag{146}$$

$$u_\phi = \sum_{n=1}^{\infty} \frac{\sin \theta P'_n}{r^{n+1}} C_{0n}, \tag{147}$$

with the surface velocities

$$u_r(r=a) = \sum_{n=1}^{\infty} \left[\frac{(n+1)A_{0n}}{2(2n-1)\eta a^n} - \frac{B_{0n}}{a^{n+2}} \right] P_n, \tag{148}$$

$$u_\theta(r=a) = \sum_{n=1}^{\infty} \left[\frac{n-2}{2n(2n-1)a^n \eta} A_{0n} - \frac{1}{a^{n+2}} B_{0n} \right] \sin \theta P'_n, \tag{149}$$

$$u_\phi(r=a) = \sum_{n=1}^{\infty} \frac{\sin \theta P'_n}{a^{n+1}} C_{0n}. \tag{150}$$

Without the azimuthal modes C_{0n} , the preceding surface velocities reduce to the form in Lighthill [40] and Blake [41]. However, notice that the coefficients A_{0n} and B_{0n} do not correspond directly to the coefficients A_n and B_n used in Lighthill [40] and Blake [41], which represent directly the radial and polar modes, respectively. With Lamb’s general solution, the radial and polar modes are represented by a combination of the A_{0n} and B_{0n} modes. The relation between the two sets of coefficients is given by

$$A_{0n} = \frac{a^n n(2n-1)\eta}{n+1} A_n - \frac{2a^n(2n-1)\eta}{n+1} B_n, \tag{151}$$

$$B_{0n} = \frac{a^{n+2}(n-2)}{2(n+1)} A_n - \frac{a^{n+2}}{n+1} B_n. \tag{152}$$

The translational and rotational velocities are computed similarly to Sect. 3.1. Without the restriction to tangential deformation, Eq. (19), the propulsion velocity becomes

$$\mathbf{U} = \frac{2}{3\eta a} \nabla [r(P_1 A_{01})] = -\frac{2}{3a\eta} A_{01} \mathbf{e}_z, \tag{153}$$

while the computation of the rotational velocity is unaffected (Eq. 32).

The flow field around an axisymmetric swimming squirmer is thus given by

$$v_r = \left(\frac{a^2}{3\eta} A_{01} - 2B_{01} \right) \frac{\cos \theta}{r^3} + \sum_{n=2}^{\infty} \frac{(n+1)P_n}{r^{n+2}} \left[\frac{A_{0n}r^2}{2(2n-1)\eta} - B_{0n} \right], \tag{154}$$

$$v_\theta = \left(\frac{a^2}{6\eta} A_{01} - B_{01} \right) \frac{\sin \theta}{r^3} + \sum_{n=2}^{\infty} \frac{\sin \theta P'_n}{r^{n+2}} \left[\frac{(n-2)r^2}{2n(2n-1)\eta} A_{0n} - B_{0n} \right], \tag{155}$$

$$v_\phi = \sum_{n=2}^{\infty} \frac{\sin \theta P'_n}{r^{n+1}} C_{0n}. \tag{156}$$

The computation of the propulsion speed of a nonaxisymmetric squirmer with radial deformation follows the same procedures as in Sect. 4.1, but without the restriction to tangential deformation, Eq. (19). The propulsion speed is given by

$$\begin{aligned} \mathbf{U} &= \frac{2}{3\eta a} \nabla \left[r \left(P_1 A_{01} + P_1^1 \cos \phi A_{11} + P_1^1 \sin \phi \tilde{A}_{11} \right) \right] \\ &= \frac{2}{3a\eta} \left(A_{11} \mathbf{e}_x + \tilde{A}_{11} \mathbf{e}_y - A_{01} \mathbf{e}_z \right), \end{aligned} \tag{157}$$

while the expression for the rotational speed remains the same, Eq. (61).

To obtain the overall swimming flow field, we follow the same procedures as in the axisymmetric case. Superimposing Lamb’s general solution in the pumping problem, Eqs. (16)–(17), with the flow fields due to the induced translation and rotation at the velocities determined earlier, we arrive at the flow field surrounding a general swimming squirmer without the assumption of purely tangential deformation:

$$v_r = \frac{1}{r^3} \left[\left(2B_{11} - \frac{a^2}{3\eta} A_{11} \right) \sin \theta \cos \phi + \left(2\tilde{B}_{11} - \frac{a^2}{3\eta} \tilde{A}_{11} \right) \sin \theta \sin \phi - \left(2B_{01} - \frac{a^2}{3\eta} A_{01} \right) \cos \theta \right] + \sum_{n=2}^{\infty} \sum_{m=0}^n \frac{(n+1)P_n^m}{r^{n+2}} \left\{ \left[\frac{A_{mn}r^2}{2(2n-1)\eta} - B_{mn} \right] \cos m\phi + \left[\frac{\tilde{A}_{mn}r^2}{2(2n-1)\eta} - \tilde{B}_{mn} \right] \sin m\phi \right\}, \tag{158}$$

$$v_\theta = -\frac{1}{r^3} \left[\left(B_{11} - \frac{a^2}{6\eta} A_{11} \right) \cos \theta \cos \phi + \left(\tilde{B}_{11} - \frac{a^2}{6\eta} \tilde{A}_{11} \right) \cos \theta \sin \phi + \left(B_{01} - \frac{a^2}{6\eta} A_{01} \right) \sin \theta \right] + \sum_{n=2}^{\infty} \sum_{m=0}^n \frac{\sin \theta P_n^{m'}}{r^{n+2}} \left\{ \left[\frac{(n-2)r^2}{2n(2n-1)\eta} A_{mn} - B_{mn} \right] \cos m\phi + \left[\frac{(n-2)r^2}{2n(2n-1)\eta} \tilde{A}_{mn} - \tilde{B}_{mn} \right] \sin m\phi \right\} + \sum_{n=2}^{\infty} \sum_{m=0}^n \frac{mP_n^m}{r^{n+1} \sin \theta} \left(\tilde{C}_{mn} \cos m\phi - C_{mn} \sin m\phi \right), \tag{159}$$

$$v_\phi = \frac{1}{r^3} \left[\left(B_{11} - \frac{a^2}{6\eta} A_{11} \right) \sin \phi - \left(\tilde{B}_{11} - \frac{a^2}{6\eta} \tilde{A}_{11} \right) \cos \phi \right] + \sum_{n=2}^{\infty} \sum_{m=0}^n \frac{\sin \theta P_n^{m'}}{r^{n+1}} \left(C_{mn} \cos m\phi + \tilde{C}_{mn} \sin m\phi \right) - \sum_{n=2}^{\infty} \sum_{m=0}^n \frac{mP_n^m}{r^{n+2} \sin \theta} \left\{ \left[\frac{(n-2)r^2}{2n(2n-1)\eta} \tilde{A}_{mn} - \tilde{B}_{mn} \right] \cos m\phi - \left[\frac{(n-2)r^2}{2n(2n-1)\eta} A_{mn} - B_{mn} \right] \sin m\phi \right\}. \tag{160}$$

Appendix C: Rate of work with radial deformation

We now compute the rate of work of a swimmer with a radial deformation. Lengthy calculations allow us to compute the integral from Eq. (76) as

$$\mathcal{P} = \frac{48\pi\eta}{a^5} \left(B_{01}^2 + B_{11}^2 + \tilde{B}_{11}^2 \right) + \frac{4\pi}{3a\eta} \left(A_{01}^2 + A_{11}^2 + \tilde{A}_{11}^2 \right) - \frac{16\pi}{a^3} \left(A_{01}B_{01} + A_{11}B_{11} + \tilde{A}_{11}\tilde{B}_{11} \right) + \sum_{n=2}^{\infty} \frac{4\pi n(n+1)}{2n+1} \left[\frac{2n^3+n^2-2n+2}{2n^2(2n-1)^2\eta a^{2n-1}} A_{0n}^2 - \frac{2(n+2)}{na^{2n+1}} A_{0n}B_{0n} + \frac{(10n+4+4n^2)\eta}{na^{2n+3}} B_{0n}^2 + \frac{(n+2)\eta}{a^{2n+1}} C_{0n}^2 \right] + \sum_{n=2}^{\infty} \sum_{m=1}^n \frac{2\pi n(n+1)(n+m)!}{(2n+1)(n-m)!} \left[\frac{2n^3+n^2-2n+2}{2n^2(2n-1)^2\eta a^{2n-1}} (A_{mn}^2 + \tilde{A}_{mn}^2) - \frac{2(n+2)}{n} (A_{mn}B_{mn} + \tilde{A}_{mn}\tilde{B}_{mn}) + \frac{(10n+4+4n^2)\eta}{na^{2n+3}} (B_{mn}^2 + \tilde{B}_{mn}^2) + \frac{(n+2)\eta}{a^{2n+1}} (C_{mn}^2 + \tilde{C}_{mn}^2) \right]. \tag{161}$$

We have again employed Eq. (78) to obtain the preceding result. Despite the presence of cross-terms, it can be shown by algebraic manipulations that the rate of work is positive definite. Removing all the nonaxisymmetric modes and transforming the coefficients with Eqs. (151) and (152), the preceding expression agrees with the results in Blake [41]. For the case of purely tangential deformation, with Eq. (19), the preceding expression reduces to Eq. (77) in the main text.

Appendix D: Squirring with arbitrary surface velocities and radial deformation

Here we allow in the general squirring profile additional radial velocity components of the form $D_m(\theta)$, $\tilde{D}_m(\theta)$,

$$u_r|_{r=a} = \sum_{m=0}^{\infty} D_m(\theta) \cos m\phi + \tilde{D}_m(\theta) \sin m\phi, \tag{162}$$

$$u_\theta|_{t=a} = \sum_{m=0}^{\infty} E_m(\theta) \cos m\phi + \tilde{E}_m(\theta) \sin m\phi, \quad (163)$$

$$u_\phi|_{r=a} = \sum_{m=0}^{\infty} F_m(\theta) \cos m\phi + \tilde{F}_m(\theta) \sin m\phi, \quad (164)$$

and follow the same matching conditions, Eqs. (83) and (84), in order to determine the coefficients A_{mn} , \tilde{A}_{mn} , B_{mn} , \tilde{B}_{mn} , C_{mn} , and \tilde{C}_{mn} in Lamb's general solution. The only difference is that we no longer have the purely tangential deformation condition (Eq. 19) and therefore are required to determine A_{mn} , \tilde{A}_{mn} , B_{mn} , \tilde{B}_{mn} such that the radial (Eq. 83) and polar (Eq. 84) matching conditions are satisfied simultaneously. Using the orthogonality of the associated Legendre polynomials and simultaneously solving the equations, we obtain

$$A_{mn} = \frac{(2n-1)a^n \eta (2n+1)(n-m)!}{2 (n+1)(n+m)!} \int_{-1}^1 \left[nD_m + \frac{\partial}{\partial \mu} (E_m \sin \theta) - \frac{m\tilde{F}_m}{\sin \theta} \right] P_n^m d\mu, \quad (165)$$

$$\tilde{A}_{mn} = \frac{(2n-1)a^n \eta (2n+1)(n-m)!}{2 (n+1)(n+m)!} \int_{-1}^1 \left[n\tilde{D}_m + \frac{\partial}{\partial \mu} (\tilde{E}_m \sin \theta) + \frac{mF_m}{\sin \theta} \right] P_n^m d\mu, \quad (166)$$

$$B_{mn} = \frac{a^{n+2} (2n+1)(n-m)!}{4 (n+1)(n+m)!} \int_{-1}^1 \left[(n-2)D_m + \frac{\partial}{\partial \mu} (E_m \sin \theta) - \frac{m\tilde{F}_m}{\sin \theta} \right] P_n^m d\mu, \quad (167)$$

$$\tilde{B}_{mn} = \frac{a^{n+2} (2n+1)(n-m)!}{4 (n+1)(n+m)!} \int_{-1}^1 \left[(n-2)\tilde{D}_m + \frac{\partial}{\partial \mu} (\tilde{E}_m \sin \theta) + \frac{mF_m}{\sin \theta} \right] P_n^m d\mu, \quad (168)$$

$$C_{mn} = \frac{a^{n+1} (2n+1)(n-m)!}{2n (n+1)(n+m)!} \int_{-1}^1 \left[-\frac{\partial}{\partial \mu} (F_m \sin \theta) - \frac{m\tilde{E}_m}{\sin \theta} \right] P_n^m d\mu, \quad (169)$$

$$\tilde{C}_{mn} = \frac{a^{n+1} (2n+1)(n-m)!}{2n (n+1)(n+m)!} \int_{-1}^1 \left[-\frac{\partial}{\partial \mu} (\tilde{F}_m \sin \theta) + \frac{mE_m}{\sin \theta} \right] P_n^m d\mu, \quad (170)$$

for $0 \leq m \leq \infty$ and $m \leq n \neq 0$. When there is no radial deformation, i.e., $D_m = \tilde{D}_m = 0$, we recover the results without radial deformation (Eqs. 90–93 and 19).

References

1. Brennen C, Winet H (1977) Fluid mechanics of propulsion by cilia and flagella. *Annu Rev Fluid Mech* 9:339–398
2. Vogel S (1996) *Life in moving fluids: the physical biology of flow*, 2nd edn. Princeton University Press, Princeton
3. Bray D (2000) *Cell movements*. Garland Publishing, New York
4. Guasto JS, Rusconi R, Stocker R (2012) Hydrodynamic phenomena in suspensions of swimming microorganisms. *Annu Rev Fluid Mech* 44:373–400
5. Lauga E, Powers T (2009) The hydrodynamics of swimming microorganisms. *Rep Prog Phys* 72:096601
6. Purcell EM (1977) Life at low Reynolds number. *Am J Phys* 45:3–11
7. Ishimoto K, Yamada M (2012) A coordinate-based proof of the scallop theorem. *SIAM J Appl Math* 72(5):1686–1694
8. Tamm SL (1972) Ciliary motion in Paramecium: a scanning electron microscope study. *J Cell Biol* 55:250–255
9. Solari CA, Ganguly S, Kessler JO, Michod RE, Goldstein RE (2006) Multicellularity and the functional interdependence of motility and molecular transport. *Proc Natl Acad Sci USA* 103(5):1353–1358
10. Fauci LJ, Dillon R (2006) Biofluidmechanics of reproduction. *Annu Rev Fluid Mech* 38:371–394
11. Galajda P, Keymer J, Chaikin P, Austin R (2007) A wall of funnels concentrates swimming bacteria. *J Bacteriol* 189(23):8704–8707

12. Di Leonardo R, Angelani L, DellArciprete D, Ruocco G, Iebba V, Schippa S, Conte MP, Mecarini F, De Angelis F, Di Fabrizio E (2010) Bacterial ratchet motors. *Proc Natl Acad Sci USA* 107(21):9541–9545
13. Denissenko P, Kantsler V, Smith DJ, Kirkman-Brown J (2012) Human spermatozoa migration in microchannels reveals boundary-following navigation. *Proc Natl Acad Sci USA* 109(21):8007–8010
14. Lauga E (2007) Propulsion in a viscoelastic fluid. *Phys Fluids* 19(8):083104
15. Fu HC, Powers TR, Wolgemuth HC (2007) Theory of swimming filaments in viscoelastic media. *Phys Rev Lett* 99:258101
16. Shen XN, Arratia PE (May 2011) Undulatory swimming in viscoelastic fluids. *Phys Rev Lett* 106:208101
17. Liu B, Powers TR, Breuer KS (2011) Force-free swimming of a model helical flagellum in viscoelastic fluids. *Proc Natl Acad Sci USA* 108(49):19516–19520
18. Pratt LA, Kolter R (1998) Genetic analysis of *Escherichia coli* biofilm formation: roles of flagella, motility, chemotaxis and type I pili. *Mol Microbiol* 2:285–293
19. Lemon KP, Higgins DE, Kolter R (2007) Flagellar motility is critical for *Listeria monocytogenes* biofilm formation. *J Bacteriol* 189(12):4418–4424
20. Houry A, Briandet R, Aymerich S, Gohar M (2010) Involvement of motility and flagella in *Bacillus cereus* biofilm formation. *Microbiology* 156(4):1009–1018
21. Berke AP, Turner L, Berg HC, Lauga E (2008) Hydrodynamic attraction of swimming microorganisms by surfaces. *Phys Rev Lett* 101:038102
22. Ramaswamy S (2010) The mechanics and statistics of active matter. *Annu Rev Condens Matter Phys* 1:323–345
23. Koch DL, Subramanian G (2011) Collective hydrodynamics of swimming microorganisms: living fluids. *Annu Rev Fluid Mech* 43:637–659
24. Berg HC (1993) *Random walks in biology*. Princeton University Press, Princeton
25. Howse JR, Jones RAL, Ryan AJ, Gough T, Vafabakhsh R, Golestanian R (2007) Self-motile colloidal particles: from directed propulsion to random walk. *Phys Rev Lett* 99:048102
26. Romanczuk P, Bär M, Ebeling W, Lindner B, Schimansky-Geier L (2012) Active brownian particles: from individual to collective stochastic dynamics. *Eur Phys J Spec Top* 202:1–162
27. Ebbens SJ, Howse JR (2010) In pursuit of propulsion at the nanoscale. *Soft Matter* 6:726–738
28. Nelson BJ, Kaliakatos IK, Abbott JJ (2010) Microrobots for minimally invasive medicine. *Annu Rev Biomed Eng* 12:55–85
29. Taylor GI (1951) Analysis of the swimming of microscopic organisms. *Proc R Soc Lond A* 209(1099):447–461
30. Reynolds AJ (1965) The swimming of minute organisms. *J Fluid Mech* 23:241–260
31. Katz DF (1974) On the propulsion of micro-organisms near solid boundaries. *J Fluid Mech* 64:33–49
32. Balmforth NJ, Coombs D, Pachmann S (2010) Microelastohydrodynamics of swimming organisms near solid boundaries in complex fluids. *Q J Mech Appl Math* 63(3):267–294
33. Gray J, Hancock GJ (1955) The propulsion of sea-urchin spermatozoa. *J Exp Biol* 32(4):802–814
34. Cox RG (1970) The motion of long slender bodies in a viscous fluids: I. general theory. *J Fluid Mech* 44:791–810
35. Batchelor GK (1970) Slender body theory for particles of arbitrary cross section in stokes flow. *J Fluid Mech* 44:419–440
36. Chwang AT, Wu TY (1971) A note on the helical movement of micro-organisms. *Proc R Soc Lond B* 178:327–346
37. Keller JB, Rubinow SI (1976) Swimming of flagellated microorganisms. *Biophys J* 16:151–170
38. Johnson RE (1980) An improved slender-body theory for stokes flow. *J Fluid Mech* 99:411–431
39. Pedley TJ, Kessler JO (1992) Hydrodynamic phenomena in suspensions of swimming microorganisms. *Annu Rev Fluid Mech* 24:313–358
40. Lighthill MJ (1952) On the squirming motion of nearly spherical deformable bodies through liquids at very small Reynolds numbers. *Commun Pure Appl Math* 109:109–118
41. Blake JR (1971) A spherical envelop approach to ciliary propulsion. *J Fluid Mech* 46:199–208
42. Ishikawa T, Simmonds MP, Pedley TJ (2006) Hydrodynamic interaction of two swimming model micro-organisms. *J Fluid Mech* 568:119–160
43. Drescher K, Leptos KC, Tuval I, Ishikawa T, Pedley TJ, Goldstein RE (Apr 2009) Dancing *Volvox*: hydrodynamic bound states of swimming algae. *Phys Rev Lett* 102:168101
44. Ishikawa T, Simmonds MP, Pedley TJ (2007) The rheology of a semi-dilute suspension of swimming model micro-organisms. *J Fluid Mech* 588:399–435
45. Ishikawa T, Pedley TJ (2007) Diffusion of swimming model micro-organisms in a semi-dilute suspension. *J Fluid Mech* 588:437–462
46. Magar V, Goto T, Pedley TJ (2003) Nutrient uptake by a self-propelled steady squirmer. *Q J Mech. Appl Math* 56:65–91
47. Magar V, Pedley TJ (2005) Average nutrient uptake by a self-propelled unsteady squirmer. *J Fluid Mech* 539:93–112
48. Michelin S, Lauga E (2011) Optimal feeding is optimal swimming for all Péclet numbers. *Phys Fluids* 23(10):101901
49. Michelin S, Lauga E (2010) Efficiency optimization and symmetry-breaking in a model of ciliary locomotion. *Phys Fluids* 22(11):111901
50. Zhu L, Do-Quang M, Lauga E, Brandt L (2011) Locomotion by tangential deformation in a polymeric fluid. *Phys Rev E* 83:011901
51. Zhu L, Lauga E, Brandt L (2012) Self-propulsion in viscoelastic fluids: Pushers vs. pullers. *Phys Fluids* 24(5):051902
52. Wang S, Ardekani A (2012) Inertial squirmer. *Phys Fluids* 24(10):101902
53. Stone HA, Samuel ADT (1996) Propulsion of microorganisms by surface distortions. *Phys Rev Lett* 77:4102–4104
54. Drescher K, Goldstein RE, Tuval I (2010) Fidelity of adaptive phototaxis. *Proc Natl Acad Sci USA* 107(25):11171–11176

55. Lamb H (1932) *Hydrodynamics*. Cambridge University Press, Cambridge
56. Brenner H (1964) The Stokes resistance of a slightly deformed sphere. *Chem Eng Sci* 19:519–539
57. Happel J, Brenner H (1973) *Low Reynolds number hydrodynamics: with special applications to particulate media*. Noordhoff International Publishing, Leyden
58. Kim S, Karilla JS (1991) *Microhydrodynamics: principles and selected applications*. Dover, New York
59. Abramowitz M, Stegun IA (1965) *Handbook of mathematical functions: with formulas, graphs, and mathematical tables*. Dover, New York
60. Jeffrey A, Zwillinger D (2007) *Table of integrals, series, and products*. Academic Press, California
61. Drescher K, Goldstein RE, Michel N, Nicolas M, Tuval I (2010) Fidelity of adaptive phototaxis. *Phys Rev Lett* 105:168101
62. Batchelor GK (1970) The stress system in a suspension of force-free particles. *J Fluid Mech* 41:545–570
63. Lighthill J (1975) *Mathematical biofluidynamics*. SIAM, Philadelphia
64. Childress S (1981) *Mechanics of swimming and flying*. Cambridge University Press, New York
65. Kim MJ, Breuer KS (2004) Enhanced diffusion due to motile bacteria. *Phys Fluids* 16(9):L78–L81
66. Turner L, Ryu WS, Berg HC (2000) Real-time imaging of fluorescent flagellar filaments. *J Bacteriol* 182:2793–2801
67. Spagnolie SE, Lauga E (2012) Hydrodynamics of self-propulsion near a boundary: predictions and accuracy of far-field approximations. *J Fluid Mech* 700:105–147